

Division of Marine Structures  
School of Naval Architecture and Marine Engineering  
National Technical University of Athens

in collaboration with

Department of Marine Technology  
Division of Offshore Structures  
Norwegian University of Science and Technology

## **MASTER THESIS**

Buckling and Ultimate Strength of Stiffened Panels

Despina Georgiou

T r o n d h e i m , N o r w a y , 2 0 1 9



Division of Marine Structures  
School of Naval Architecture and Marine Engineering  
National Technical University of Athens

Department of Marine Technology  
Division of Offshore Structures  
Norwegian University of Science and Technology

**MASTER THESIS**

Buckling and Ultimate Strength of Stiffened Panels



**MASTER THESIS**

Buckling and Ultimate Strength of Stiffened Panels

**Manolis Samuilidis**

(Co-supervisor)

**Jørgen Amdahl**

(Co-supervisor)

**Konstantinos Anyfantis**

(Assistant Professor)

.....



## **Acknowledgements**

The master thesis is part of Master Program “Marine Technology” of the Department of Naval Architects and Marine Engineers, National Technical University of Athens. It has been conducted in collaboration with the Norwegian University of Science and Technology, Department of Marine Technology (Center of Autonomous Marine Operations & Systems), during a five-month Erasmus mobility program.

I could not omit my sincere regards to all these people who contributed educationally, advisory and emotionally, for the completion of my master thesis. So, first of all, I would like to express my heartfelt thanks to my supervisors, Pr. Manolis Samuilidis (NTUA) and Pr. Jørgen Amdahl (NTNU), for their invaluable advices and suggestions, as well as for their encouragement and support in the writing of this work. The continuous and systematic supervision and excellent cooperation at all stages of the thesis motivated me to give my best for this project. I feel obliged to thank Lars Brubak, Eivind Steen from DNV GL, for providing me with the necessary information during the process of work. Finally, I would like to thank K. Anyfantis, for our discussions over various engineering aspects.

It would certainly not be possible for me to fail to express my gratitude to my family for the continuous and beneficial support that contributes to the achievement of my goals. Obviously, a thank you is not enough to pay back the support I have received over the years. I hope that they look worthy of their expectations.



## Contents

Scope .....	1
<b>1. Introduction .....</b>	<b>3</b>
<b>2. Fundamental Theory and Analysis Methods to Simulate Buckling Behavior .....</b>	<b>5</b>
a. Buckling Collapse Behavior of Stiffened Panels .....	6
2.2 Buckling Collapse Behavior of Stiffeners .....	7
2.3 Overall Buckling versus Plate Buckling.....	8
2.3.1 Minimum Flexural Rigidity to Avoid Overall Buckling .....	8
2.3.2 Effective width during Buckling .....	9
2.4 Analytical Solutions for Torsional Buckling of Stiffeners.....	10
2.4.1 Nonuniform Torsion of Thin-walled Bars of Open Cross Section.....	11
2.4.2 Torsional Buckling .....	12
2.4.3 Interaction between Plate and Stiffener.....	13
2.5 Buckling Strength.....	15
2.5.1 Local Buckling Strength of Stiffened Plate Considering Web-Plate Interaction ...	16
2.5.2 Interactive Buckling Strength.....	17
<b>3. Finite Element Analysis on Buckling.....</b>	<b>19</b>
3.1 General .....	19
3.2 Model Geometry, Material Properties and Mesh .....	20
3.3 Loading Cases .....	21
3.4 Boundary Conditions for Buckling Modes.....	23
3.5 Linear and Nonlinear analysis on FEA.....	26
3.5.1 Linear FEA .....	26
3.5.2 Nonlinear FEA.....	29
<b>4. Proposed Rules and Regulations.....</b>	<b>33</b>
4.1 Buckling Capacity .....	33
4.1.1 Overall Stiffened Panel Capacity Check .....	34
4.1.2 Plate Buckling Capacity Check .....	34
4.2. Stiffener Buckling Capacity Check .....	36
4.2.1 Ultimate buckling capacity .....	36
4.2.2 Torsional buckling capacity .....	38
<b>5. Results from Assessment Methods.....</b>	<b>43</b>
5.1 General .....	43
5.2 Panels with Attached T-stiffeners .....	43
5.2.1 Panel T-400 .....	45
5.2.2 Panel T-600 .....	54

5.2.3 Panel T-900 .....	60
5.2.4 Proposal Verification with FEA .....	68
5.3 Panels with Attached Flatbars .....	69
5.3.1 Finite Element Analysis of Flatbars .....	69
5.3.2 Ultimate Buckling Capacity of Flatbars .....	75
6. Conclusions .....	77
References .....	81

## **Scope**

Present Rules given by Classification Societies (IACS) give rational criteria for dimensioning the hull structure ensuring sufficient strength for safe operations. However, the ship designers/yards are in fierce competition and by offering reduced steel weight, possible increased cargo capacity and reduce fuel consumption can be achieved. This business pressure leads to creative thinking among designers and more optimal and thinner structures are the result. For extreme loads this again will challenge the structural capacity limits and unwanted “overload” damages and permanent sets may be the result.

Safe Rule scantlings are mainly determined by stress and buckling criteria such as given in DNV GL Ship Rules. They are typically based on text book formulas (Euler, etc.) modified to take into consideration different buckling modes, interactions between elements, non-linear behaviour, combined bi-axial/shear loads acting, etc. These types of Rule models are termed Closed Form Method (CFM) and covers basically all relevant failure modes. Though, some of these CFM models have limitations, and improvements/extensions are needed to provide for more consistent dimensioning for some designs.

The most advanced approach is to use non-linear FE tools (Abaqus or equivalent). Such models are expensive and time consuming to analyse and not much used in normal ship design work unless the case requires special documentation. However, such models are very valuable for benchmarking simpler buckling models.

The task of the master thesis work is to assess existing buckling models of stiffened plate as proposed by DNV GL and develop new and improved models where found necessary. The buckling/failure modes to be considered are torsional buckling of different types of stiffener sections and global (overall) buckling of stiffened panels.

The approach used for solving the overall task will constitute a combination of analytical work and numerical analyses using non-linear FE tool. Analytical work will be needed in relation to derivation of closed formed buckling models and proposal of approximations while numerical buckling analyses (Abaqus) will be used for validating the simpler formulas (CFM)

The work reviews and summarizes the DNV GL (IACS) Rules, as relevant for the two buckling modes to be considered. Additionally, numerical comparison studies (Abaqus) were

carried out for validating the CFM predictions given above. Two levels of validation achieved. The first refers to the comparison of eigenvalues and the second, on ultimate capacity over a relevant parameter span as typical for ship designs (vary stiffener lengths, plate thickness, etc.). Finally, alternative models were improved or developed for eigenvalues for torsional and overall buckling strength.

## **1. Introduction**

Thin plates are structural elements that are widely used in many engineering fields, such as aerospace, shipbuilding and civil engineering. Ribbed and stiffened ship plates, offshore, and aerospace panels are commonly utilized and always subjected to partial edge traction on their own plane. This type of loading can induce buckling, which negatively affects the function of the structural elements concerned. Plate instability is generated globally or locally through in plane compression and lateral loading. The corrugations resulting from plate instability may cause permanent deformations and reduce the efficiency of the entire structure.

The project focuses on buckling and ultimate strength of stiffened panels. Torsional buckling of the stiffeners, plate local buckling as well as overall buckling of stiffened panels will be examined. During the assessment of their structural responses, both numerical and analytical methods will be implemented.

Elastic buckling stresses are defined as the stress lever over which an abrupt increase in the lateral configuration of the structure is remarked. After elastic buckling load is reached, equilibrium becomes unstable and the structure loses its ability to support additional loadings without experiencing excessive deformations. Therefore, the largest force which may be applied to the structure is reached and it either breaks or begins to carry less load. When considering elasto-plastic behavior, ultimate load is the maximum load carrying capacity, and tracing it to the equivalent cross-sectional area of the stiffened panel, the ultimate stress or strength of the material can be extracted.

The goal of the study is to determine the ultimate buckling strength of various stiffened panels under a series of parametric/numerical studies. In the end, the behavior of the structure will be assessed, based on chosen cross-sectional geometries and certain loading conditions, helping to understand the model's structural behavior when it follows an unstable path. These results will give prominence to the most efficient cross-sectional design based on the ultimate capacity check of the structure, before its overall collapse due to torsion occurs.

To begin, the following chapter attempts an overview of the existing literature, by analyzing the principal theories developed by Bleich, Timoshenko, Owes, etc. The theoretical background contains a short description of plate and stiffener buckling behavior individually and, afterwards, a more detailed expatiation on torsional buckling follows. The developed equations explain torsional and lateral buckling of beams with open cross-sections, which simulate a cross-section of a plate with an attached stiffener. Additionally, the basic formulas

referring to plate/stiffener interaction are highlighted, in order to comprehend the correlation of each structural member on the ultimate behavior of a stiffened panel.

In the third chapter, the variables of the finite element model are defined. Geometrical and material properties, meshing, boundary conditions and applied loading scenarios implemented for all stiffener sections are set up. Afterwards, a description of finite element analysis procedure takes place, by the explanation of linear and nonlinear method. During linear analysis, the extraction the appropriate eigenvalues is explained, attaining an initial prediction of possible collapse modes. The eigenmodes shall correspond to the introduced geometrical imperfections during nonlinear analysis. Finally, Riks force/displacement control process is mentioned, justifying the reason this algorithm is the most efficient for the estimation of the model's ultimate deformations.

The forth chapter, aims to validate the proposed formulas by IACS, for the calculation of torsional buckling capacity of stiffened panels. An overall review of the demanded plate and stiffener buckling capacity checks is presented, followed by a detailed description of the components constituting torsional buckling capacity formula. The contribution of each parameter on ultimate capacity is examined, in order to assess formula's effectiveness for different stiffener profiles.

Continuing, the fifth chapter makes an extended presentation of the numerical results of FEA for T-stiffeners and flatbars. In the beginning, the selection procedure from a range of different eigenmodes, arising from various load cases and geometries, shows how plate and stiffener failure modes are superimposed during nonlinear analysis. These modes, combined with material nonlinearity and proportionally increased loadings will lead to the ultimate buckling capacity evaluation. The extracted results will be compared, between similar stiffeners of various geometries, so as to assess how the dimensions of a stiffener effects its torsional stiffness. In the end, the verification of the numerical analysis with the proposed formulas will validate the accuracy of such modifications.

Finally, the last chapter provides an overall summary of the arisen results during the project work. The utilized evaluation methods, numerical and analytical, are assessed on their accuracy and inclusiveness. The variable parameters of FEA, like stiffener section type and geometrical dimensions, combined with different load cases, define the response of a stiffened panel and effect the magnitude of maximum stresses that can bear. Additionally, it is concluded that T-stiffeners respond in a different manner than flatbars, a fact that in some cases the proposed analytical formulas fail to capture.

## 2. Fundamental Theory and Analysis Methods to Simulate Buckling Behavior

The minimum structural unit in a stiffened plate is the plate, partitioned by longitudinal and transverse stiffeners. This plate is in general rectangular and is considered to be simply supported along its four sides. Actually, when this plate buckles and lateral deflection develops, the stiffeners along four sides resist against the rotation of the plates. So, exactly saying, such rectangular plate is elastically supported along its four sides. However, the constraint by the stiffeners is considered weak in general, and the rectangular plate is assumed to be simply supported along its four sides.

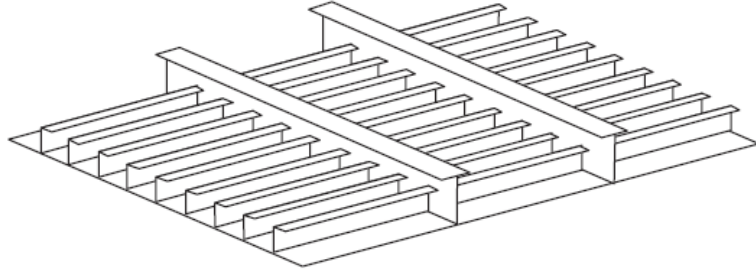


**FIG. 2.1**

Ship structure composed of stiffened plates

In the actual structure, isolated plate does not exist, but a rectangular plate is a part of continuous plating as indicated in Fig.

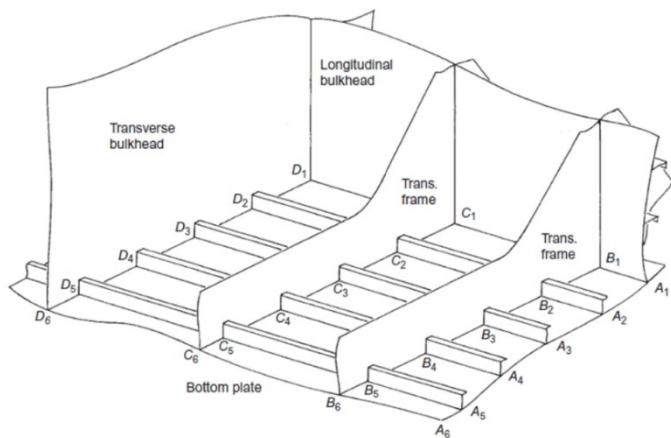


**FIG. 2.2**

Bottom ship stiffened plate

## 2.1 Buckling Collapse Behavior of Stiffened Panels

The stiffened plate is considered with stiffeners of the same size with equal distances. Compressive load is acting in the direction of the stiffeners. If the stiffeners have enough flexural stiffness and little deflect under the action of thrust load, the plate locally buckles and the stiffeners do not buckle, Fig. 2.3A. In this case, local buckling mode of the plate is expressed as:

$$w_{long} = A_{mn} \sin \frac{m\pi x}{a} \sin \frac{n\pi y}{B} \quad (2.1)$$

where m and n are the numbers of half wave of the local buckling mode in longitudinal and transverse directions,  $a$  the transverse edge and  $B$ , the length of the panel.

On the other hand, when thrust load acts on the same plate but in transverse direction, local buckling of a different mode occurs. as indicated in Fig. 2.3B when the stiffeners are stiff enough. The local buckling mode in this case is one half-wave mode between stiffeners, and is expressed as follows:

$$w_{transv} = A_{1n} \sin \frac{\pi x}{a} \sin \frac{n\pi y}{B} \quad (2.2)$$

Contrary to these, when the stiffeners are not stiff enough, overall buckling takes place as indicated in Fig. 2.3C. In this case, buckling mode is in one half-wave mode regardless of the direction of compressive load, whether it is in longitudinal or in transverse direction. Therefore:

$$w_{overall} = A_{11} \sin \frac{\pi x}{a} \sin \frac{\pi y}{B} \quad (2.3)$$

In addition to the above, overall buckling often takes place as the secondary buckling after the local buckling has occurred as the primary buckling in the case of a stiffened plate; see Fig. 2.3D. The buckling mode is expressed as the sum of Eq. (2.1 to 2.3).

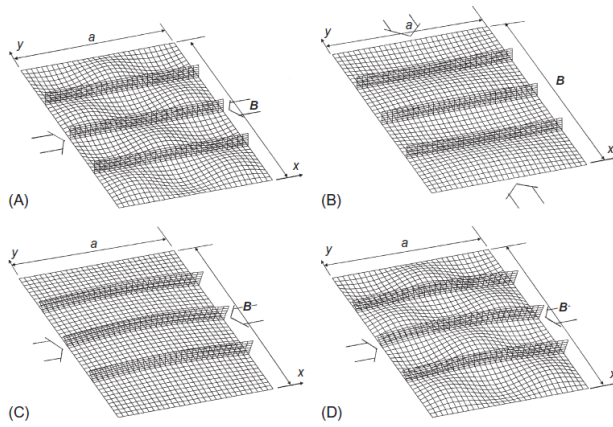


**FIG. 2.3**

Buckling mode of stiffened plate under compression: (A) Local buckling (longitudinal thrust). (B) Local buckling (transverse thrust). (C) Overall buckling. (D) Overall buckling after local buckling

## 2.2 Buckling Collapse Behavior of Stiffeners

There are several possible buckling modes of stiffeners predominantly under thrust, as shown in Fig. 2.4. The lateral torsional buckling, Fig. 2.4A, is a rotation of stiffeners about a plate-stiffener connection line. For slenderer stiffeners such as a flat-bar stiffener, more localized buckling, called tripping, Fig. 2.4B, likely takes place and often interacts with the local panel buckling. For the combination of a slender web with a relatively stiff flange, a local web buckling, Fig. 2.4C may take place also accompanied by the interaction with plate. It is a common design philosophy for stiffeners that the local panel buckling must be preceded by these stiffener buckling. When overall buckling, Fig. 2.4C takes place, deflection of a stiffener located at  $y = yi$  is expressed as:

$$w_{si} = A_{11} \sin \frac{\pi x}{a} \sin \frac{\pi y_i}{B} \quad (2.4)$$

The torsional behavior of the stiffeners remains a critical condition that will occupy the margin of that project. Cases in which a column will buckle either by twisting or by a combination of bending and twisting could be proved fatal for the undergoing structure. The torsional rigidity of the structure defines to the most the ultimate buckling path that will result.

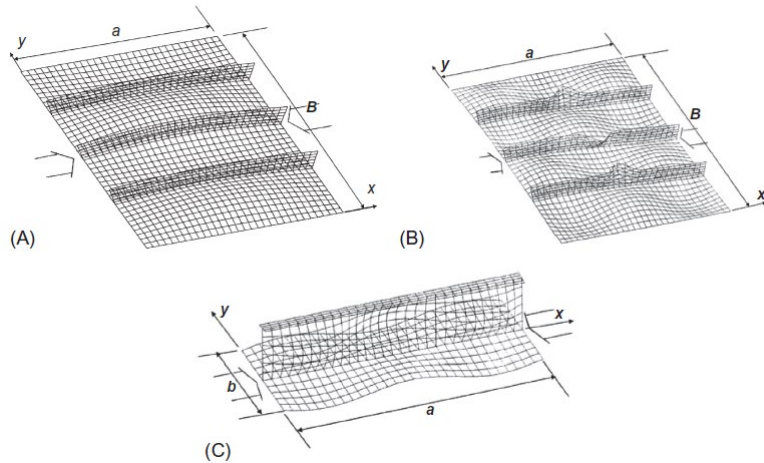


**FIG. 2.4**

Buckling mode of stiffener in stiffened plate. (A) Lateral torsional buckling. (B) Tripping. (C) Web buckling.

In the following, theories and methods focused on torsional buckling analysis of stiffened panels will be briefly introduced.

## 2.3 Overall Buckling versus Plate Buckling

### 2.3.1 Minimum Flexural Rigidity to Avoid Overall Buckling

The minimum rigidity of longitudinal stiffeners necessary to ensure that overall buckling does not precede plate buckling has been investigated by various authors (Cox & Riddel, 1949; Seide, 1953; Timoshenko & Gere, 1961).

For a panel containing one and two equally spaced longitudinal stiffeners, Bleich (1952) presented approximate formulas. The minimum required rigidity is expressed in terms of a parameter  $\gamma_x$ , which is the ratio of the flexural rigidity of the combined section to the flexural rigidity of the plating, expressed by the moment of inertia of a section,  $I_x$ , comprised of a stiffener together with a width  $b$  of plate.

$$\gamma_x = \frac{EI_x}{Db} = \frac{12(1-\nu^2)I_x}{bt^3} \quad (2.5)$$

The panel aspect ratio  $\Pi$  is expressed in respect to the panel length  $L$ , which in the case of a panel with one longitudinal stiffener equals to  $a$ .

$$\Pi = \frac{L}{B} = \frac{a}{B} \quad (2.6)$$

The area ratio  $\delta_x$ , in which  $A_x$  is the cross-sectional area of the stiffener is:

$$\delta_x = \frac{A_x}{bt} \quad (2.7)$$

Cox and Riddel (1949), based on Bleich's formulas, investigated plates with up to three stiffeners, and their analysis is capable of extension of more stiffeners. They investigated the smallest size of stiffeners necessary to prevent overall buckling of a flat panel before buckling of the plate between stiffeners. Furthermore, the effect of torsional stiffness of the stiffeners is included. The analysis was done using a strain energy method and the solution was given in closed form.

A more general solution valid for any number of stiffeners has been presented by Klitchieff (1951). Therefore, the minimum value of  $\gamma$  to ensure that stiffener buckling does not precede plate buckling is given by the following formula:

$$(\gamma_x)_{min} = \delta_x (1 + N_\beta^2 \Pi^2)^2 + \frac{4}{\pi} \Pi (1 + N_\beta^2 \Pi^2) \sqrt{2 + N_\beta^2 \Pi^2} \quad (2.8)$$

where  $N_\beta$  the number of panels= 1 + number of longitudinal stiffeners

### 2.3.2 Effective width during Buckling

Since slender panels are normally designed such that plate buckling precedes overall buckling, when the latter occurs, the plate flange of the stiffener will not be fully effective over the width  $b$ . Instead, it is necessary to take some reduced effective width,  $b_e$ .

The effective width caused by buckling has long been a vexed question, mainly because in most cases it was being discussed and applied in the difficult context of the ultimate strength of panels that were not slender and therefore did not buckle elastically. For elastic or near-elastic buckling, a satisfactory formula was derived by von Karman, Sechler and Donnell (1932).

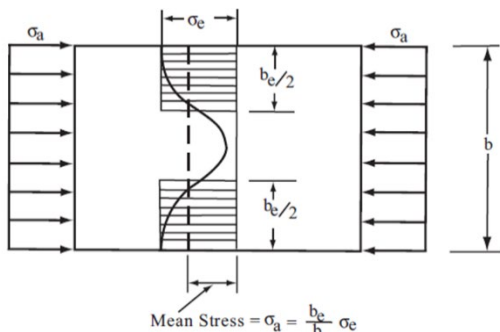


**FIG. 2.5**

Postbuckling stress distribution –effective width

They idealized the state of stress within the buckled plate by assuming that, because of buckling, the center portion has no compressive stress, while the edge portions of the plate remain fully effective and carry a uniform stress  $\sigma$  (Fig. 2.5). In other words, the buckled center portion is discounted completely and the original plate of width  $b$  is replaced by a narrower unbuckled plate of effective width  $b_e$ . Then, both widths are connected with the relation:

$$\sigma_e = \frac{b}{b_e} \sigma_a \quad (2.9)$$

While buckling grows progressively, effective plate is always on the verge of further buckling. Thus, the effective width is taken to be the width at which the equivalent plate would buckle at an implied stress of  $\sigma_e$ .

$$\sigma_e = k \frac{\pi^2 D}{b_e^2 t} \quad (2.10)$$

and because for the original plate  $(\sigma_a)_{cr} = k \frac{\pi^2 D}{b^2 t}$  and  $k$  is assumed to be the same in both cases:

$$\frac{b_e}{b} = \sqrt{\frac{(\sigma_a)_{cr}}{\sigma_e}} = 1.9 \frac{t}{b} \sqrt{\frac{E}{\sigma_e}} \quad (2.11)$$

for  $k = 4$  and  $\nu = 0.3$ .

When  $\sigma_e$  reaches yield stress, effective width reaches its minimum value:

$$(\frac{b_e}{b})_{min} = \frac{1.9}{\beta} \quad (2.12)$$

where  $\beta$  is plate slenderness parameter.

However, if the panel is truly slender, overall buckling would in most cases occur before  $\sigma_e$  reaches  $\sigma_Y$ , therefore eq.2.11 is utilized as a general expression.

## 2.4 Analytical Solutions for Torsional Buckling of Stiffeners

Timoshenko and Gere (1963), developed a general theory of elastic stability, focusing on buckling conditions that call for consideration the stability of a structure. During that, the torsional buckling behavior of thin-walled cross sections under various boundary conditions were investigated.

The extent of torsional buckling pattern depends on configuration of the cross-section of stiffeners as well as loading conditions. When the stiffener has a symmetric cross-section such as a flatbar or a tee-bar, its rotation owes to the symmetrical deflection in plating.

On the contrary, when an angle-bar stiffener is attached, cross-section of the stiffener is not symmetrical. When lateral pressure loads act, the force corresponding to lateral pressure passes through the shear center of the stiffener's cross-section, which is the intersecting point of mid-thickness lines of the web and the flange. In this case, if the stiffener is free, only translation takes place. However, the stiffener is attached to the plate and intersection line of the plate and the stiffener cannot move sideways.

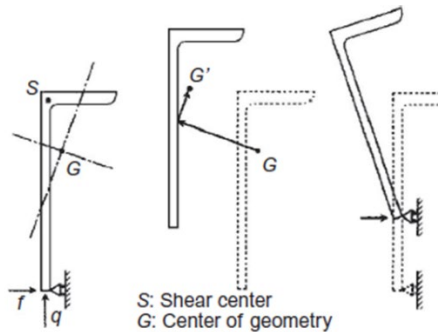


**FIG. 2.6**

Displacement and rotation of angle bar stiffener

#### 2.4.1 Nonuniform Torsion of Thin-walled Bars of Open Cross Section

In the case of nonuniform torsion of any cross section, axial strain at its longitudinal fibers develops. The principal conditions that favor that procedure are based on the nonuniform distribution of torque along the length of the bar, as well as to the fixity of one cross section's side.

The differential equation describing that applies to any bar of thin-walled open cross section and is expressed as:

$$M_t = C \frac{d\varphi}{dz} - C_1 \frac{d^2\varphi}{dz^3} \quad (2.13)$$

where  $\varphi$  is the angle of twist

$C = GJ = \frac{1}{3} Gmt^3$  is the torsional rigidity of the bar of shearing modulus of elasticity  $G$  and thickness  $t$ .

$C_1$  is the warping rigidity of the section

and  $C_1 = E * C_w$ , with the quantity  $C_w$  called the warping constant.

For cross-sectional shapes consisting of thin rectangular elements which intersect at a common point the warping constant  $C_w$  can be taken equal to zero.

The torque  $M_t$  of eq.2.5 is balanced partially by shearing stresses due to pure torsion and partially by the resistance of the flanges to bending. The first component of the above expression is proportional to the rate of change of the angle of twist along the axis of the beam, call the Saint Venant torsion moment. The latter considers the bending of the flanges, neglecting the effect of shearing forces in the flanges on the curvature and implementing only the effect of normal stresses.

## 2.4.2 Torsional Buckling

There are cases in which a thin-walled bar subjected to uniform axial compression will buckle torsionally while its longitudinal axis remains straight. When symmetry conditions apply at two of the axes of the cross section ( $x, y$ ), the axis of the bar remains straight, while each flange buckles by rotating about the other one ( $z$  axis). In order to determine the compressive force which produces torsional buckling, it is necessary to consider the deflection of the flanges during buckling.

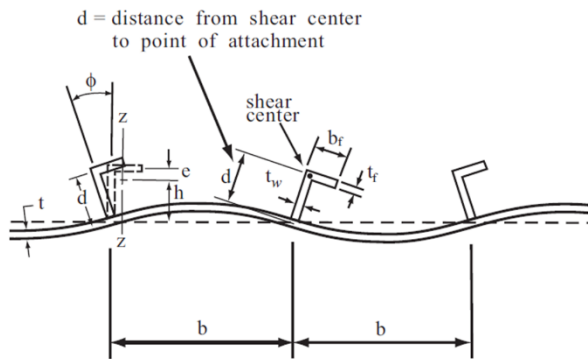


**FIG. 2.7**

Stiffener tripping

The differential equation of torsional buckling is based on eq. 2-5, for any shape of cross section as long as the shear center and centroid coincide.

$$C_1 \frac{d^4 \varphi}{dz^4} - (C - \sigma_a I_0) \frac{d^2 \varphi}{dz^2} + K_\varphi \varphi = 0 \quad (2.14)$$

where  $I_0$  is the polar moment of inertia of the stiffener about the center of rotation

$K_\varphi$  the distributed rotational restraint which the plating exerts on the stiffener

and  $\sigma_\alpha$  the elastic tripping stress, that could cause tripping according to elastic theory

If the ends of the stiffener are regarded as simply supported, the solution for  $\varphi(x)$  is a buckled shape in which the rotation  $\varphi$  varies sinusoidally in  $m$  half-waves over the length  $a$ . The elastic tripping stress will be denoted as  $\sigma_{\alpha,T}$ . From the foregoing equation, it may be seen that  $\sigma_{\alpha,T}$  is the minimum value of  $\sigma_\alpha$  that satisfies the following, in which  $m$  is a positive integer.

$$C_1 d^2 \frac{m^4 \pi^4}{\alpha^4} - (C - \sigma_\alpha I_0) \frac{m^2 \pi^2}{\alpha^2} + K_\varphi (\sigma_\alpha, m) = 0 \quad (2.15)$$

Under this type of load, the stiffener acts essentially as a column, but its tripping or torsional buckling differs from that of a column because the rotation occurs about the line of attachment to the plating. Furthermore, the plate itself offers some restraint against rotation and if the plating is sturdy there will be some distortion of the stiffener due to web bending.

#### 2.4.3 Interaction between Plate and Stiffener

In the absence of other factors, the rotational restraint  $K_\varphi$  offered by the plating comes directly from the plate's flexural rigidity, which causes in response to the rotation  $\varphi$  of the stiffener, a total distributed restraining moment  $M_R = 2M$ , along the line of the stiffener attachment (see fig.2.8). If the individual plate panels are long, then the aspect ratio effects are ignored and by considering a unit strip of plating across the span  $b$ , it may be shown that  $\varphi = \frac{1}{2} Mb/D$ . Thus, the rotational restraint coefficient is:

$$K_\varphi = \frac{M_R}{\varphi} = \frac{4D}{b} \quad (2.16)$$

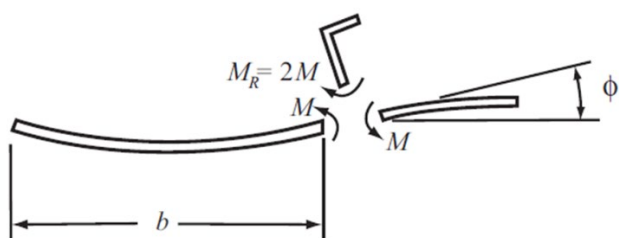
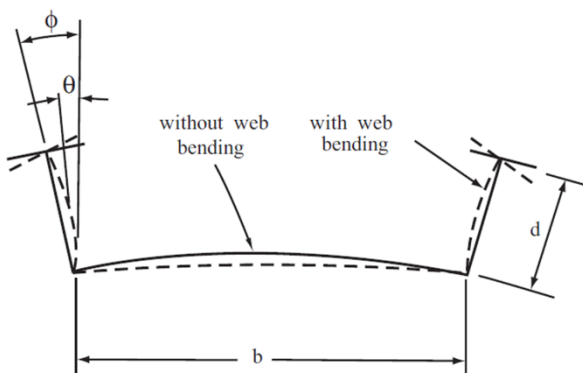


FIG. 2.8

Restraining moment exerted by plating

However, this assumes that the buckled displacement of the stiffener is entirely due to rigid body rotation. This is only accurate if the flexural rigidity of the stiffener web is much larger than that of the plate. In practice, some of the sideways displacement of the stiffener flange occurs because of bending of the web, and this effect becomes important if the plating is sturdy or if the stiffener web is slender.

Next figure shows the deflected shape when web bending does and does not occur, for the same amount of maximum sideways displacement of the stiffener flange.



**FIG. 2.9**

Effect of web bending

The rotational restraining moment exerted by the plate is proportional to the angle of rotation of the plate along the line of attachment. It may readily be shown that the two angles are related by:

$$\theta = C_r \varphi \quad (2.17)$$

$$\text{where } C_r = \frac{1}{1 + \frac{2}{3} \left( \frac{t}{t_w} \right)^3 \frac{d}{b}}$$

$C_r$  is the factor by which the plate rotational restraint is reduced because of web bending.

The effect of plate aspect ratio may be accounted for by applying another correction factor  $C_a$  (Sharp, 1966):

$$K_\varphi = \frac{4D}{b} C_r C_a \quad (2.18)$$

$$\text{where } C_r = \frac{1}{1 + 0.4 \left( \frac{t}{t_w} \right)^3 \frac{d}{b}} \quad (2.19)$$

$$\text{and } C_a = 1 + \frac{m^2}{a^2}, \text{ for } \sigma_\alpha = 0$$

Expressing factor  $C_a$  as a function of  $\sigma_\alpha$ ,  $m$  and  $a$ , calculates a systematic set of values of a plate stiffness factor that accounts for both aspect ratio and buckling effects (Kroll, 1943). In this expression,  $\sigma_\alpha$  is the applied stress and  $\sigma_0$  the plate buckling stress.

$$C_a = 1 - \left( \frac{2\sigma_\alpha}{\sigma_0} \right) \frac{m^2}{a^2} \quad (2.20)$$

As buckling stress levels are approached, the factor  $C_a$  and as an extension the plate rotational restraint  $K_\varphi$ , become proportional to the quantity  $1 - (m - a)^2$ . If the plate panel between the stiffeners is long or at least square, it will buckle in a number of square subpanels, approximately  $a$ . In most cases, the number will exceed the number of half waves of the stiffener tripping mode  $m$ , and in such cases the plate buckling has a little deleterious effect on  $K_\varphi$ . On the other hand, if the plate buckling pattern matches that of the stiffener ( $a = m$ ), then the plate loses its ability to provide any rotational restraint.

For stiffened panels of usual proportions tripping occurs in a single half wave,  $m = 1$ , hence it is mainly square or short panels in which this loss of stiffness can occur. Evidently, plate rotational restraint is formed:

$$K_\varphi = \frac{4D}{b} \left[ \frac{1}{1 + 0.4(\frac{t}{t_w})^3 \frac{d}{b}} \right] \left[ 1 - \left( \frac{2\sigma_\alpha}{\sigma_0} \right) \frac{m^2}{a^2} \right] \quad (2.21)$$

In stiffened panels of average proportions, the critical tripping mode is  $m = 1$ . Of course, this cannot be simply assumed, but the correct value must be ascertained in each case. The only exception to this is the calculation of a lower bound solution, in which the plating rotational restraint is deliberately ignored and the critical mode is always  $m = 1$ .

To sum up, tripping involves three variables,  $\sigma_\alpha$ ,  $m$ ,  $a$ , that are interrelated in a rather complex fashion. The critical value of  $\sigma_\alpha$  depends on  $K_\varphi$  and  $m$ , while  $m$  depends on the magnitude of  $K_\varphi$  and  $K_\varphi$  depends on both  $\sigma_\alpha$  and  $m$ .

## 2.5 Buckling Strength

The elastic buckling strength of a plate subjected to various loads can be expressed as follows:

$$\sigma_{cr} = \frac{\pi^2 k E}{12(1-\nu^2)} \left(\frac{t}{b}\right)^2 \quad (2.22)$$

where  $t$  and  $b$  are the thickness and the breadth of the plate, respectively. On the other hand,  $k$  is buckling coefficient, which is determined depending on loading and boundary conditions. Here, buckling strength of a rectangular plate with various boundary conditions is considered under uniaxial compression.

The buckling coefficient,  $k$ , is expressed as:

$$k = \left( \frac{a}{mb} + \frac{mb}{a} \right)^2 \quad (2.23)$$

where  $a$  and  $b$  are the length and the breadth of the plate and  $m$  corresponds to the number of half-waves of a buckling mode. Therefore, the deflection is:

$$w = A_m \sin \frac{m\pi x}{a} \sin \frac{\pi y}{b} \quad (2.24)$$

### 2.5.1 Local Buckling Strength of Stiffened Plate Considering Web-Plate Interaction

Stiffened plates are so designed that local panel buckling takes place before overall buckling occurs. For the design of such a stiffened plate, the buckling coefficient,  $k$ , is usually taken as 4.0. However, local buckling strength of a stiffened plate is affected by the interaction between plate and stiffener web, and is expected to increase. To account for the influence of the interaction between the plate and the stiffener web accurately, the stiffener web has to be treated as a plate.

Continuous stiffened plate as illustrated in Fig. 2. is considered. On the plate, stiffeners of the same size are fitted with equal distances. The interaction between the plate and the stiffener web can be simulated by assuming the following deflection modes as buckling modes (Fujikubo M, Yao T).

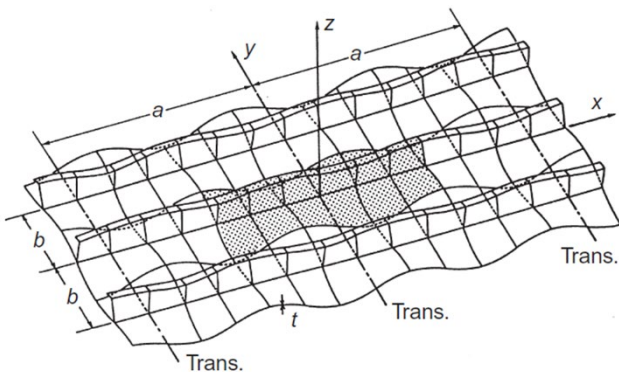


**FIG. 2.10**

Continuous stiffened plate

For plate:

$$w = \sin \frac{m\pi x}{a} \left\{ W_1 \sin \frac{\pi y}{b} + \frac{1}{2} W_2 (1 - \cos \frac{2\pi y}{b}) \right\} \quad (2.25)$$

The first term represents the buckling mode of a simply supported plate and the second term that of a clamped plate. The latter term produces bending moment which is transferred to the stiffener web.

For stiffened panel:

$$w_{web} = \sin \frac{m\pi x}{a} \left\{ V_1 \frac{z}{h} + V_2 (1 - \cos \frac{\pi z}{2h}) + V_3 \sin \frac{\pi z}{2h} \right\} \quad (2.26)$$

Three deflection components of a stiffener web are considered. The first term represents a rigid-body rotation about the line of attachment of stiffener web to plate. The second term produces the bending moment transferred to the panel and the third term that to the stiffener flange from the stiffener web.

## 2.5.2 Interactive Buckling Strength

The evaluation of the local panel buckling strength considering the interaction between the plate and the stiffener web as well as that between stiffener web and flange is of major interest. In the case of a continuous stiffened plating, symmetry conditions can be imposed along the centerlines in both longitudinal and transverse directions. So, it is enough if the buckled region partitioned by four centerlines is analyzed instead of analyzing the whole stiffened plating.

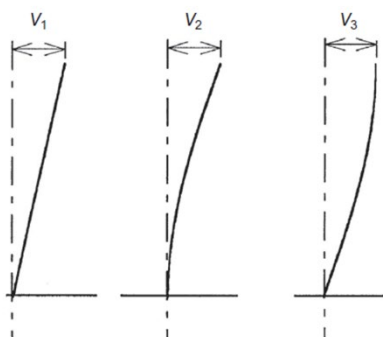


**FIG. 2.11**

Assumed deflection components in stiffener web.

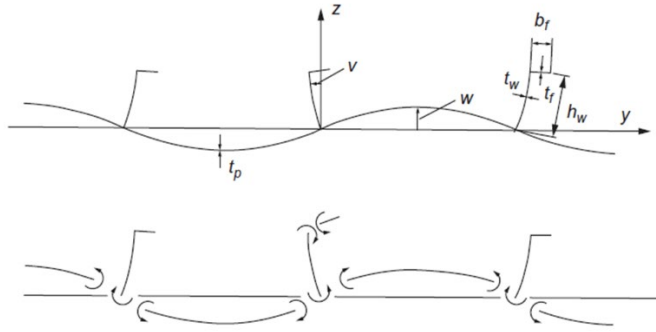


**FIG. 2.12**

Equilibrium condition and deflection mode.

\

The following boundary conditions are considered in the formulation:

- 1) Continuity condition for rotation angle along panel/web intersection (for  $y=z=0$ )

$$\frac{\theta w}{\theta y} = \frac{\theta u_{web}}{\theta z}$$

- 2) Equilibrium condition for bending/torsional moment along panel/web intersection (for  $y=z=0$ )

$$D_w \left( \frac{\theta^2 u_{web}}{\theta z^2} + \nu \frac{\theta^2 u_{web}}{\theta x^2} \right) + 2D_p \left( \frac{\theta^2 w}{\theta y^2} + \nu \frac{\theta^2 w}{\theta x^2} \right) = 0$$

$$\text{where } D_w = \frac{Et_w^3}{12(1-\nu^2)}, \quad D_p = \frac{Et_p^3}{12(1-\nu^2)}$$

and  $t_p$  and  $t_w$  are the thicknesses of panel and stiffener web.

- 3) Equilibrium condition for bending/torsional moment along web/flange intersection of stiffener considering continuity of rotation (for  $z=h$ ).

$$GJ_f \frac{\theta^3 u_{web}}{\theta x^2 \theta z} - D_w \left( \frac{\theta^2 u_{web}}{\theta z^2} + \nu \frac{\theta^2 u_{web}}{\theta x^2} \right) = 0$$

where  $GJ_f$  is the torsional stiffness of the flange of a stiffener.

### **3. Finite Element Analysis on Buckling**

#### **3.1 General**

The finite element method is a common approach for structural analysis in general, and especially for marine structures, as they are often complex structures subjected to a wide range of loads. Most structural problems are too complex to be solved by classic analytical methods, which could be significantly time-consuming. For this reason, numerical analysis can be proved more efficient, approaching at a large extent analytical and giving accurate results immediately. Nevertheless, FEA should be considered only as a practical tool, thus the extracted results must be checked and assessed continuously, always combined with engineering experience and correct interpretation.

There are several commercially available preprocessing software tools on the market, which can be utilized to generate the desired model for the subsequent analysis. For the implementation of that project, the modeling and the finite element analysis of the various stiffened panels, the chosen software was ABAQUS FEA package, versions 6.11 and 6.14-1. More specifically, ABAQUS/CAE was used for both the 3D-modeling and analysis (pre-processing) and visualization of the finite element analysis results. A subset of ABAQUS/CAE, including only the post-processing module, was launched independently in ABAQUS/Viewer product.

Aiming to assess the torsional buckling behavior and consequently the ultimate capacity of stiffened panels, two analyses had been held. Firstly, a linear analysis (eigenvalue analysis), which estimates elastic buckling capacity of an “ideal” stiffened panel and demonstrates its emerging buckling modes and, secondly, a non-linear analysis for the estimation of the ultimate buckling capacity of an “imperfect” stiffened panel. FE models are usually expensive and time consuming to analyze and not much used in normal ship design work, unless the case requires special documentation. However, such models are very valuable for benchmarking simpler buckling models.

Scantling design of the stiffened panels is one of the most important and challenging tasks through the entire structural design process. “Scantling” refers to the determination of geometrical dimensions of a structural component/system. During the analysis, stiffeners of various profiles and geometry (web height/width, stiffener spacing/span, etc.) and different loading conditions (pure axial, biaxial, lateral) has been examined. Although the applied boundary conditions remained mostly similar, some cases demanded inevitable modifications, in order to reflect real conditions.

### 3.2 Model Geometry, Material Properties and Mesh

Each stiffened panel consists of five stiffeners spread in transverse direction, with a total panel width of  $B = (n + 1) * S$ , where  $n$  is the number of stiffeners and  $S$  the span between two stiffeners. In the longitudinal direction a three-span model has been used, with a span switch of  $A = \frac{1}{2}L + L + L + \frac{1}{2}L$  along the plate length.

As a convention, longitudinal/axial, transverse and vertical directions correspond to x, y and z axes respectively.

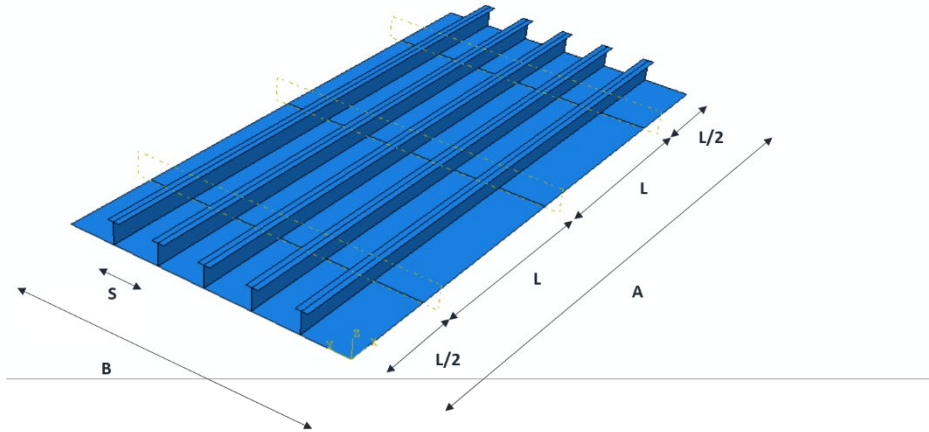


**FIG. 3.1**

Module of the plate with the attached longitudinal stiffeners

Panels with torsionally weak stiffeners of two types are introduced: flatbar and T-section stiffeners. Length remains fixed, while height and thickness change. During the parametric study, the correlation of the torsional rigidity between the plate and the stiffeners will be fulfilled.

Marine engineering steel is mainly used for ships and offshore oil drilling platforms. More specifically, the specimen is made of structural high-strength marine steel of type S315, a conventional yield strength steel. The Young's modulus (modulus of elasticity),  $E$ , is 210 GPa, Poisson's ratio,  $\nu$ , is 0.3 and material is isotropic. The width of the steel plate is between 4200-4800 mm, the length is 9600mm and the thickness is 22 mm. Web's height varies from 300-1000 mm and thickness from 12-20 mm for T-stiffeners and 250-400mm height and 20mm thickness for flatbars. When T-stiffeners attached, their flange has a width of 200 mm and 22 mm thickness.

The module is separated in three principal structural components: the plate, the web and the flange. Each one is separately defined in assembly, assigned to different geometrical dimensions and has been matched to different load magnitudes. In the case of flatbars, the flange does not exist.

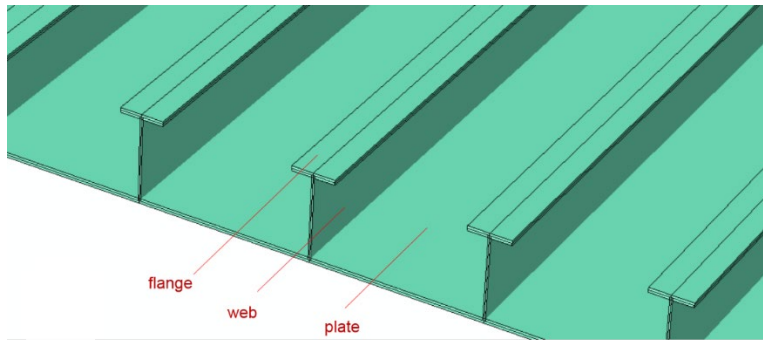


**FIG. 3.2**

**Principal components of a stiffened panel**

The whole model was discretized by S8R type elements of 50\*50 mm size. That kind of mesh is quite dense, leading to highly accurate estimations of stresses and displacements, combined with sufficient processing time. The S8R element is an eight-node, doubly curved shell element, with six degrees of freedom at each node (three displacement and three rotation components). Since a shell element can be curved, the normal to the shell surface is defined in each node separately. Furthermore, the element allows changes in the thickness as well as finite membrane strain.

For the analysis shell elements were utilized because of the thickness of the structural elements, which is comparatively smaller than the other two dimensions. Additionally, other types of elements, like solid elements, would perform a stiffer bending behavior, leading to divergence from analytical solution. Finally, shell elements consume less computational time, establishing them more time efficient.

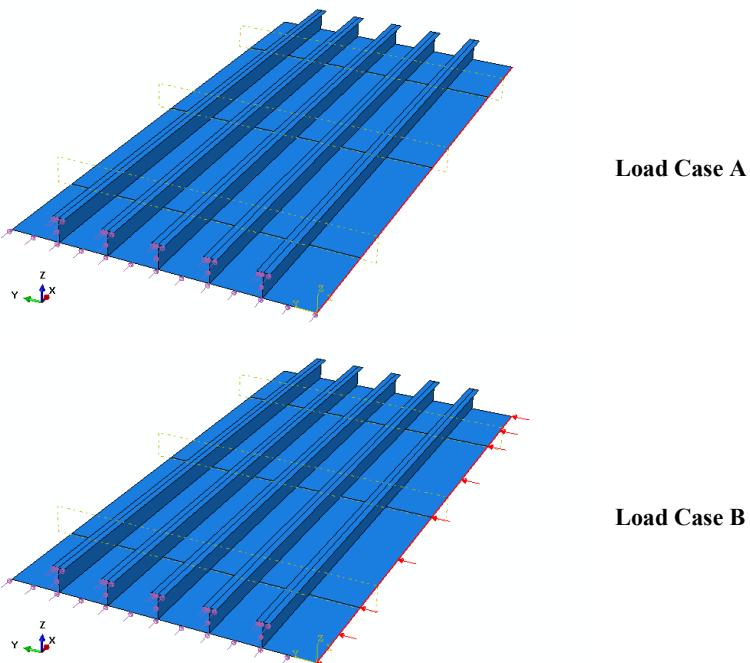
### **3.3 Loading Cases**

Buckling is an ultimate limit state condition (ULS) caused by compression of the principal members of a structure. What interests most in buckling behavior is the deformations caused under proportionally increasing compressive loads until the collapse of a structural part.

Due to the complexity of the applied loads, it is common to examine more simplified loading scenarios. Gradually, a combination of those simple loadings could contribute on the final stress assessment. During the project the basic loading cases applied to the model are:

- Case A – Pure axial compression: Proportionally increasing compressive stresses applied vertically on the module's short edge, ( $\sigma_1$ ).
- Case B – Biaxial compression: Proportionally increasing compressive stresses applied vertically on two consequent edges of the module, ( $\sigma_1, \sigma_2$ ). The stress ratio of the long to the short edge,  $\psi$ , will range for values of 10% – 40%.
- Case C – Combined biaxial and lateral compression: In the case of biaxial compression (Case B), a moderate pressure of 0.6 MPa at the bottom surface of the plate will be added. That pressure level corresponds to a 60-meter water height, taking into consideration some dynamic loads as well.

Attention should be paid when defining the applied lateral pressure. That could be achieved either by increasing it proportionally until reaching its maximum magnitude or by setting it as a predefined load at the beginning. Evidently, the latter reflects more accurately real conditions, nonetheless the deviances between the two approaches could explain how engineering judgement determines correct problem design.



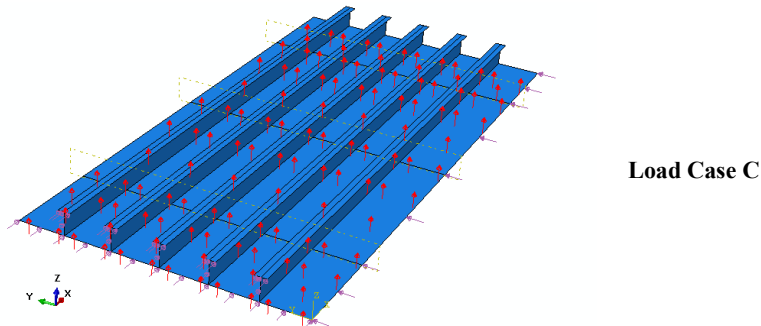


**FIG. 3.3**

Applied loads - Cases A, B, C

The notation utilized for each FEA model includes the type of loading, dominant boundary conditions at the web/plate longitudinal intersection and the edge stress ratio (when existing).

<b>SR</b>	Single load - Restrained BC	Case A
<b>CR10</b>	Combined loads – Restrained BC transverse load =10% of axial load	Case B
<b>CR20</b>	Combined loads – Restrained BC transverse load =20% of axial load	Case B
<b>CR40</b>	Combined loads – Restrained BC transverse load =40% of axial load	Case B
<b>CF40L</b>	Combined loads – Restrained BC – Lateral pressure transverse load =40% of axial load	Case C

**TABLE 3.1**

Notation for each FEA model

To maintain a uniform stress level over the whole edge surface, the compressive stresses should be deduced in respect with the thickness of the assigned edge. Thus, a unit stress level was assigned to plate's surface, which was defined as the reference surface, and the rest loads were derived proportionally to that reference.

### 3.4 Boundary Conditions for Buckling Modes

It is obvious that a successful approach of real conditions encountered on the majority of ship's bottoms and offshore structures depends on the accurate simulation of the model's boundaries. The existing boundary conditions and constraints shall be such that the structural

element can be checked for its torsional buckling capacity. Consequently, the imposed BC shall simulate pure torsional buckling conditions, determining the module's design loads.

Four sets of boundary conditions were introduced corresponding to the plate edges; two for the transverse ends and two for the longitudinal.

One transverse edge is imposed to a compressive uniform axial stress in the longitudinal direction, simulating the principal source of buckling. On that side, both the plate and the stiffener shall be free to translate in all planes and simultaneously the y-z plane be maintained vertical. Thence, an equation has been set in plate's edge surface nodes forcing them to move as a rigid body in axial direction. Stiffeners should be able to deform, so rotation through x-axis is free, but in order to maintain symmetry conditions at the ends of the panel rotation through the other two axes should be constrained.

On the opposite transverse side, the model shall comply with the same boundary conditions. Additionally, a restriction in the horizontal direction is prevailed to resist the force acting on the loaded short edge.

Concerning the longitudinal edges, the condition of clamped edges should be approached by allowing in plane moves of the boundaries but fixed vertical displacements. All nodes of the loaded longitudinal edge should move together in y-direction, therefore an equation for the second degree of freedom is utilized. In order to avoid local buckling along edges all rotations shall be suppressed. When biaxial loading is active, the unloaded longitudinal edge is restrained in transverse direction as a resistance on the transverse load.

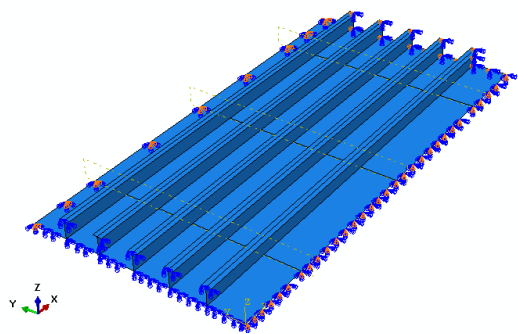


**FIG. 3.4**

Dominant boundary conditions at the edges of the module

Of a great interest is the state in the intersection of the plate and the stiffeners longitudinally, as well as in the intersection of the stiffeners and the transverse girders.

In the first place, to simulate a pure torsional buckling effect on the stiffeners, vertical displacements on the nodes of the web/plate intersections were constrained. For this reason, the lines connecting the five webs with the plate were fixed in z-direction, thus suppressing interframe flexural stiffener buckling. However, this is a fictional condition that does not reciprocate in real cases, where these parts are practically free to move and deform in all planes. It is self-evident that when applying lateral pressure at the bottom of the panel, that constraint shall be removed.

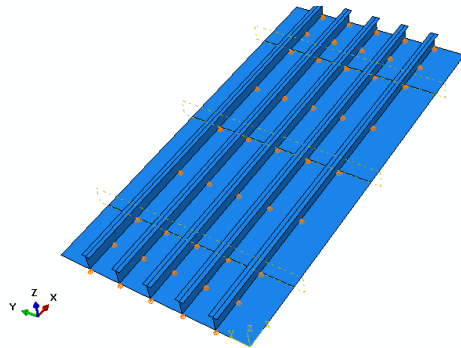


**FIG. 3.5**

Vertical restrain of the web/plate intersection

Transverse girders were not included physically in the model, nonetheless their effect on stiffener's boundary conditions were modeled. The simulation of their lateral support on the stiffeners along distinct lines designed with boundary conditions obtained in their junction. These stiff transverse frames contribute in the distribution of shearing stresses dominating on the web frames due to loading of the plate. Binding the vertical movement of the web at these points prevents shearing forces from straining the stiffener, as well as local failure. Simultaneously, the webs at these positions should remain straight but also free to move in transverse direction. By introducing an equation constraint to all web's heightwise nodes, so that they move in respect with the corresponding nodes at the bottom in the transverse direction, this relative motion preserves the rigidity of the intersection. It should be clarified that for stiffeners having a flange, it is independent of girder/web correlation, having the freedom to translate/rotate in all directions. Modelling of the transverse girders would give more realistic support and consequently more accurate buckling capacity results, but these restraint effects are not influencing sufficiently on rule predictions and thus could be omitted.

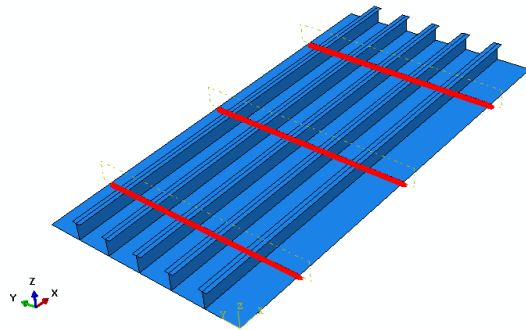


**FIG. 3.6**

Restraint of vertical motion in the intersection of the transverse girders and the stiffeners

### 3.5 Linear and Nonlinear analysis on FEA

Buckling occurs as an instability when a structure can no longer support the existing compressive load levels. Many structural components are sufficiently stiff that they will never suffer any form of instability. In practice it is the relationship between radius of gyration and length that is the deciding factor and hence long span girders of heavy section could easily be clear of any instability mode. This type of structure would only fail in compression by local yielding if load levels can reach that extreme.

At the other extreme, structures that are slender could fail at load levels well below what is required to cause compressive yielding. The failing mode tends to be toward the classic Euler buckling mode. For long thin rods and struts the Euler buckling calculation can be quite accurate. The buckling here is of a bifurcation type — there is a rapid transition from axial loading response to a lateral response, which is usually catastrophic.

A very large number of structures fall into the intermediate category where the Euler buckling calculation is not very accurate and can tend to seriously overestimate the critical buckling load. The transition to instability is more gradual in this category. The structure is able to carry increasing loads, with perhaps changes in deformed shape and plasticity, until a maximum (or limit) load is reached. At this point instability occurs. This may be catastrophic, or the structure may transition to a new mode shape that can carry further load.

#### 3.5.1 Linear FEA

Eigenvalue buckling analysis is the first step during the structural stability verification of a module. It is a linear perturbation procedure, which measures its imperfection sensitivity

under acting compressive loads. Generally, it is used to estimate the critical buckling loads of “stiff” structures, during which we consider an “ideal” structure with no material and geometry nonlinearities.

Stiff structures carry their design loads primarily by axial or membrane action rather than by bending action. Their response usually involves very little deformation prior to buckling. A simple example of a stiff structure is the Euler column, which responds very rigidly to a compressive axial load until a critical value is reached. After this point it bends suddenly and exhibits a much lower stiffness. However, even when the response of a structure is nonlinear before collapse, a prior eigenvalue buckling analysis can provide useful estimates of the regions prompt to have stability issues, presents how close to stability failure is and highlights expected collapse mode shapes.

### Eigenvalue problems applied on structural stability

For the eigenvalue prediction, an incremental loading pattern is defined by an arbitrary magnitude, that will be scaled by the load multipliers/eigenvalues,  $\lambda_i$ , found in the eigenvalue problem. The scope is to define the critical or bifurcation load for which the model’s stiffness matrix becomes singular, if nontrivial solution exists.

$$Ax = \lambda x$$

$$(A - \lambda I)x = 0 \quad (3.1)$$

where  $x$  = eigenvector,  $\lambda$  = eigenvalue

According to Invertible Matrix Theorem, solving  $\lambda$  in the former equation is equivalent of finding that  $\lambda$  for which the matrix  $(A - \lambda I)$  becomes singular (not invertible). Consequently, its determinant shall become zero and the eigenvalues of the matrix  $A$  can be solved from the equation:

$$\det(A - \lambda I) = 0 \quad (3.2)$$

Correlating previous equations to a beam case, the stiffness matrix connects the applied load to the resulting deformation. In a situation where the stiffness matrix,  $K$ , is singular, no load is demanded to move the structure into an unstable configuration.

$$Kp = P \quad (3.3)$$

where  $K$  = stiffness matrix,  $p$  = displacement vector,  $P$  = load vector

The buckling loads are calculated relative to the base state of the structure, that is the current state of the model. Therefore, the base state can include preloads or “dead loads”, although in most cases of classical eigenvalue buckling problems preloads are zero. In the last case, the stiffness matrix can be divided into an elastic part and a nonlinear, load dependent part.

$$K = K_E + K_G \quad (3.4)$$

where  $K_E$  = elastic, linear part of stiffness matrix,

$K_G$  = geometric, nonlinear, load dependent part of the stiffness matrix

Since the geometric part of the stiffness matrix,  $K_G$ , is nonlinear dependent on the applied load, it is necessary to linearize the problem. ABAQUS implements the stability problem through secant formulation. Here,  $K^{t0}$  represents the stiffness matrix before the start of the current analysis and  $K^{t1}$  represents the stiffness matrix of the first load step.

$$K = K^{t0} + \lambda(K^{t1} - K^{t0}) \quad (3.5)$$

By solving the determinant of the stiffness matrix,  $K^t$ , the critical load factors,  $\lambda_{cr}$ , can be found.

$$\det(K^{t0} + \lambda(K^{t1} - K^{t0})) = 0 \quad (3.6)$$

After critical buckling loads are defined, the lowest value of load multipliers is of main interest. That is, the lowest magnitude of loading that will cause significant deformations on the shape of the structure, inducing its collapse. However, the emerging buckling shapes are only normalized vectors with maximum displacement component equal to 1.0, thus do not represent actual magnitudes of deformation. If all displacement components are zero, the maximum rotation component is normalized to 1.0. These buckling mode shapes are often the most useful outcome of the eigenvalue analysis, since they predict the likely failure mode of the structure.

### The eigenvalue extraction method

Abaqus/Standard offers the Lanczos and the subspace iteration eigenvalue extraction methods. The Lanczos method is generally faster when a large number of eigenmodes is required for a system with many degrees of freedom. The subspace iteration method may be faster when only few eigenmodes are demanded.

For the purposes of this project, frequently was inevitable to search through a large number of modes, in order to distinguish local plate buckling and torsional buckling of the stiffeners at its purest version. These eigenmodes were not necessarily encountered at the first buckling modes, therefore having a wide range of critical modes, allowed to choose the most appropriate. This was the reason that Lanczos method established as the most efficient.

After eigenvalue analysis, the efficient selection of the critical failure modes is indissolubly dependent on the implementation of the proposed imperfections. However, often eigenmodes do not demonstrate a pure version and the selection of the appropriate modes is not straightforward, but requires detailed and careful judgement.

### 3.5.2 Nonlinear FEA

In real structures, the ideal behavior, as proposed by Euler's approach is not applicable. A nonlinear analysis demonstrates a nonlinear relation between applied forces and displacements. Nonlinear effects can originate from geometrical nonlinearities (i.e. large deformations), material nonlinearities (i.e. elasto-plastic material) and contact. These effects result in a stiffness matrix which is not constant during the load application, opposed to the linear static analysis, where the stiffness matrix remained constant. As a result, a different solving strategy is required and therefore a different solver.

In general, the solving procedure evolves the appropriate eigenmodes extracted from linear analysis, that are going to be used as initial imperfections of the model. Utilization of the appropriate algorithms implemented by nonlinear analysis lead to the estimation of ultimate buckling capacity and the edge shortening of the model.

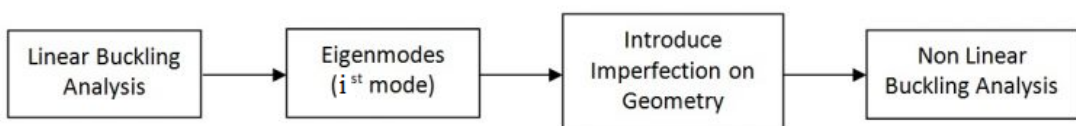


**FIG. 3.7**

Algorithm of nonlinear analysis

Modern analysis software makes it possible to obtain solutions to nonlinear problems. However, experienced skill is required to determine their validity and these analyses can easily be inappropriate. Care should be taken to specify appropriate model and solution

parameters. Understanding the problem, the role played by these parameters and a planned and logical approach will do much to ensure a successful solution.

### Geometrical Nonlinearity

In analyses involving geometric nonlinearity, changes in geometry as the structure deforms are considered in formulating the constitutive and equilibrium equations. Many engineering applications require the use of large deformation analysis based on geometric nonlinearity, whereas small deformation analysis based on geometric nonlinearity is required for some applications, like analysis involving shells.

A major problem is to quantify and motivate the amount of imperfection that has to be included in the analysis. For this aim an imperfection sensitivity analysis has to be carried out. In the figure below, it is possible to see the effect of imperfections in contrast to an ideal buckling path; including imperfections reduces the buckling load of a structure (the secondary path has no imperfections).

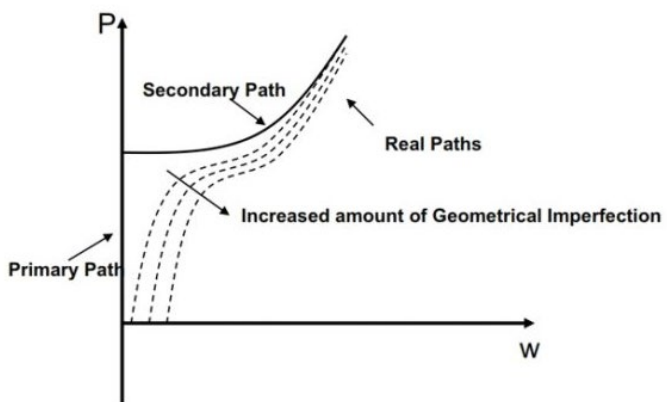


**FIG. 3.8**

Imperfection sensitivity analysis

Fabricated stiffened panels that are commonly used for ships and offshore structures include geometrical nonlinearities, and a perfect shape can hardly be achieved. In the model, geometric nonlinearities were implemented through the several buckling shapes that were exported during eigenvalue analysis. As mentioned previously, these correspond more accurately to plate local buckling and stiffeners torsional buckling. Afterwards, the maximum factorized displacements on each eigenvector were superimposed to “produce” the final geometrically imperfect shape.

## **Material Nonlinearity**

Material nonlinearity involves the nonlinear behavior of a material based on a current deformation, deformation history, rate of deformation, temperature, pressure, and so on. Examples of nonlinear material models are large strain (visco) elasto-plasticity and hyperelasticity (rubber and plastic materials).

The examined stiffened panels are composed of marine structural steel S315, with a yield stress of 315 MPa. As it seems from figure 3.9 , the material follows a linear behavior until reaching its yield stress, attaining small deformations. After that point, it begins following a nonlinear path, effecting also its deformation pattern. The certain curve shall be utilized for describing the material properties of the model.

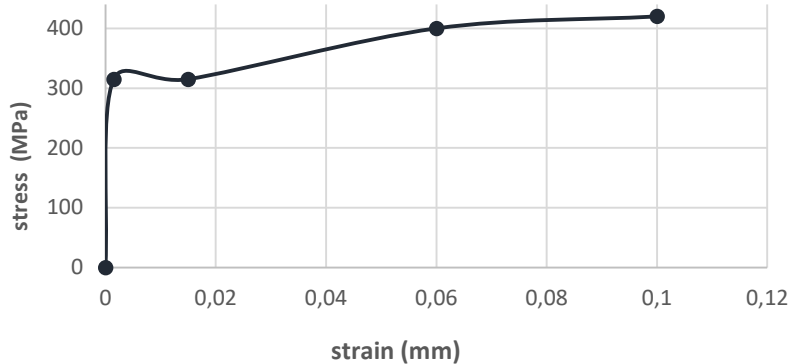


**FIG. 3.9**

Stress – strain curve of S315 steel.

## **Postbuckling Analysis**

During the analysis a range of results referring to the interrelation between the dominant loading conditions and the actual modification of the geometry that the model could perform are provided. Of special interest is the edge shortening of the stiffened panel under various influences.

For the postbuckling study the Riks iteration method is used, providing information about the proportionally increasing stresses acting on a structure and the corresponding displacements

of the elements that constitute it. It is a variant of the Arc Length method, but unlike the Newton-Raphson method, this method uses an extra constraint and allows the solver to reach the convergence with lower applied load and find the equilibrium. This property of the Riks method makes it possible to trace the behavior after a limit point is reached, even though the stiffness matrix is not positive definite. The Newton method can also work as a solution scheme when accomplishing postbuckling analysis, but only with the requirement that the postbuckling path is stable. While this is hard to know in advance, the Riks method is recommended for this kind of analysis because of its validity for both stable and unstable behavior of the postbuckling paths.

According to Abaqus manual, the loading during a step in the Riks solution scheme is always proportional to the current load magnitude:

$$P_{tot} = P_0 + \Gamma(P_{ref} - P_0) \quad (3.7)$$

Where  $P_0$  is the buckling load (where the instability initiates),  $P_{ref}$  is the reference load, and  $\Gamma$  is the Load Proportionality Factor (LPF).

Postbuckling can be divided into two different types, stable and unstable postbuckling. The characteristic of stable postbuckling behavior is that the structure continues to carry the load that it is subjected and maintains its stiffness, having a positive definite stiffness matrix (see Figure ). On the contrary, unstable postbuckling occurs when the structure loses its stiffness and is no more able to carry the same amount of load. This often leads the structure to start undergoing very large geometrical changes for decreased or even unchanged loading, (see Figure, case b).

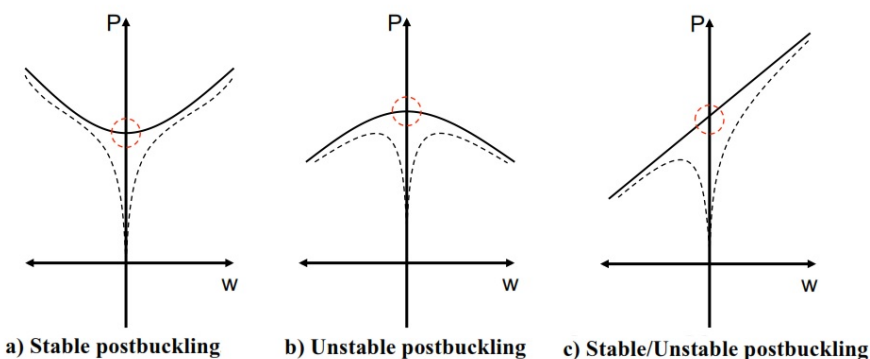


**FIG. 3.10**

Postbuckling path behavior

## **4. Proposed Rules and Regulations**

Present Rules given by International Association of Classification Societies (IACS) gives rational criteria for dimensioning the hull structure ensuring sufficient strength for safe operations. However, the ship designers/yards are in fierce competition and by offering reduced steel weight, possible increased cargo capacity and reduce fuel consumption can be achieved. This business pressure leads to creative thinking among designers and more optimal and thinner structures are the result. For extreme loads this again will challenge the structural capacity limits and unwanted “overload” damages and permanent sets may be the result.

Safe Rule scantlings are mainly determined by stress and buckling criteria such as given in DNV GL Ship Rules. They are typically based on text book formulas (Euler, etc.) modified to take into consideration different buckling modes, interactions between elements, non-linear behaviour, combined bi-axial/shear loads acting, etc. These types of Rule models are termed Closed Form Method (CFM) and covers basically all relevant failure modes. Though, some of these CFM models have limitations, and improvements/extensions are needed to provide for more consistent dimensioning for some designs.

Below, a revised version regarding buckling capacity of the stiffeners and more specifically stiffener warping stress is being proposed by DNV GL. For a detailed interpretation of the review, the proposal is displayed at references.

### **4.1 Buckling Capacity**

This section focuses on the calculation of buckling capacities for structural members like the plate and the stiffeners. Buckling failure modes which are mainly excessive deformation, torsion, warping, translational and/or rotational displacement, are specified in the Rules through design criteria, to prevent or control the deformation from compromising the integrity of the structure.

In order to prevent the occurrence of those failure modes, several criteria shall be fulfilled. The basic ultimate buckling capacity criteria that should be checked refer to:

- Overall stiffened panel capacity
- Plate capacity
- Stiffener capacity

Below, the two first criteria will be mentioned briefly and only stiffener capacity check will be developed in full detail.

#### 4.1.1 Overall Stiffened Panel Capacity Check

The limit state is based on both the elastic column and torsional buckling behaviors of a simple beam subjected to equivalent axial forces and lateral loads.

$$\frac{P_z}{c_f} = 1$$

The above check suggests that the nominal lateral load acting on the stiffener due to applied stresses,  $P_z$ , should be equalized by the elastic support provided by the stiffener,  $c_f$ .

#### 4.1.2 Plate Buckling Capacity Check

Plate capacity under combined in-plane loads must fulfil the following formulas:

$$\left( \frac{\gamma_{c1}\sigma_x S}{\sigma_{cx}'} \right)^{e_0} - B \left( \frac{\gamma_{c1}\sigma_x S}{\sigma_{cx}'} \right)^{e_0/2} \left( \frac{\gamma_{c1}\sigma_y S}{\sigma_{cy}'} \right)^{e_0/2} + \left( \frac{\gamma_{c1}\sigma_y S}{\sigma_{cy}'} \right)^{e_0} + \left( \frac{\gamma_{c1}|\tau|S}{\tau_c'} \right)^{e_0} = 1$$

$$\left( \frac{\gamma_{c2}\sigma_x S}{\sigma_{cx}'} \right)^{2/\beta_p^{0.25}} + \left( \frac{\gamma_{c2}|\tau|S}{\tau_c'} \right)^{2/\beta_p^{0.25}} = 1 \quad \text{for } \sigma_x \geq 0$$

$$\left( \frac{\gamma_{c3}\sigma_y S}{\sigma_{cy}'} \right)^{2/\beta_p^{0.25}} + \left( \frac{\gamma_{c3}|\tau|S}{\tau_c'} \right)^{2/\beta_p^{0.25}} = 1 \quad \text{for } \sigma_y \geq 0$$

$$\frac{\gamma_{c4}|\tau|S}{\tau_c'} = 1$$

in which applied normal and shear stresses,  $\sigma_x$ ,  $\sigma_y$  and  $\tau$  are connected with ultimate buckling normal and shear stresses  $\sigma_{cx}$ ,  $\sigma_{cy}$  and  $\tau_c$ .

#### Elastic Buckling Reference Stresses

The elastic buckling reference stresses describe the local buckling stress level dominating at each section of the stiffened panel. A separate estimation for the plate and the stiffener will be

made, depending on the loading conditions at the edges of each component. In the presence of flange, individual calculations for the web and the flange are made, in order to correlate their contribution to the final buckling capacity.

The elastic buckling reference stress of the plate, in  $N/mm^2$ , is independent of stiffener type and remains the same for all cases:

$$\sigma_{E\_P} = \frac{\pi^2 E}{12(1 - \nu^2)} \left(\frac{t_p}{b}\right)^2 K_p \quad (4.1)$$

Where,  $t_p$ , is the thickness of the plate and  $b$ , is the width of the plate. The buckling factor,  $K_p$ , is estimated in accordance to the boundary conditions performing on the plate and depends on the aspect ratio,  $\alpha$ , and the edge stress ratio,  $\psi$ , as shown in Table 3 (Index 1). Assuming that simply supported edges is the most representative boundary condition for plate edges in a high level of accuracy, yet not completely,  $K$  is (IACS PT PH32, Table 3, Case 1):

$$K_p = F_{long} \frac{8.4}{\psi + 1.1} \quad (4.2)$$

Simply supported edges of an unstiffened panel have a correction factor given as  $F_{long} = 1$  and for uniform axial loading in the longitudinal direction,  $\psi = 1$ .

When flatbars are used as stiffeners, the elastic buckling reference stress, in  $N/mm^2$ , is:

$$\sigma_{E\_fb} = \frac{\pi^2 E}{12(1 - \nu^2)} \left(\frac{t_w}{h_w}\right)^2 K_{fb} \quad (4.3)$$

where  $t_w$  is the thickness of the web and  $h_w$  its height. The buckling coefficient factor,  $K_s$ , is considered as a simply supported plate at three edges and free at the top edge (IACS PT PH32, Table 3, Case 3).

$$K_{fb} = \frac{4(0.425 + \frac{1}{\alpha^2})}{3\psi + 1} \quad (4.4)$$

In the case of a T-stiffened panel, the elastic buckling capacity of the web and the flange shall be examined separately. It is important to address the restriction that the flange provides to the web, in order to protect it from failure. Otherwise, if the flange buckles in its own plane, it would reach its capacity level and could not provide any restriction to the web anymore.

Due to the presence of the flange at the top side, the web could be considered as a plate simply supported on all edges (IACS PT PH32, Table 3, Case 1). The elastic buckling reference stress of the web is calculated like in the case of an unstiffened plate:

$$\sigma_{E\_web} = \frac{\pi^2 E}{12(1 - \nu^2)} \left(\frac{t_w}{h_w}\right)^2 K_{web} \quad (4.5)$$

$$K_{web} = F_{long} \frac{8.4}{\psi+1.1} \quad (4.6)$$

The difference now is that the thickness of the web is considered as the reference thickness and the plate provides a restraint to the web. Thus:

for  $\frac{t_p}{t_w} > 1$ ,  $c = 0.3$  and

$$F_{long} = c + 1 = 1.3$$

The flange is considered as a beam and thus, its elastic buckling reference stress is calculated:

$$\sigma_{E\_fl} = \frac{\pi^2 E I_y}{A l^2} \quad (4.7)$$

where  $I_y = \frac{t_f b_f^3}{12}$  the moment of inertia around the strong axis and  $A = t_f * b_f$ , the cross sectional area of the flange.

A comparison of these two reference stresses demands web over flange capacity, so that the former could withstand the loads of the latter.

## 4.2. Stiffener Buckling Capacity Check

### 4.2.1 Ultimate buckling capacity

The ultimate buckling capacity of the stiffeners is to be checked in respect to the effective axial stress acting on the stiffener with its attached plating,  $\sigma_a$ , the bending stress on the stiffener,  $\sigma_B$  and the warping stress,  $\sigma_w$ , according to the following interaction formula:

$$\frac{\gamma_c \sigma_a + \sigma_B + \sigma_w}{R_{EH}} S = 1$$

where  $R_{EH}$  the specified minimum yield stress of the material.

In the above formula, the stress caused due to torsional deformation is defined as:

$$\sigma_w = E y_w \left( \frac{t_f}{2} + h_w \right) \Phi_0 \left( \frac{\pi}{l} \right)^2 \left( \frac{1}{1 - \frac{\gamma \sigma_a}{\sigma_{ET}}} - 1 \right) \quad \text{for the stiffener} \quad (4.8)$$

$$\sigma_w = 0 \quad \text{for the plate}$$

where  $y_w$  the distance, in mm, from centroid of stiffener cross section to the free edge of stiffener flange, to be taken as:

$$y_w = \frac{t_w}{2} \quad \text{for flat bar}$$

$$y_w = b_f - \frac{h_w t_w^2 + t_f b_f^2}{2 A_s} \quad \text{for angle and bulb profiles}$$

$$y_w = b_{f-out} + 0.5 t_w - \frac{h_w t_w^2 + t_f (b_f^2 - 2 b_f d_f)}{2 A_s} \quad \text{for L2 profile}$$

$$y_w = b_{f-out} + 0.5 t_w - \frac{(h_w - t_f) t_w^2 + t_f (b_f + t_w)^2}{2 A_s} \quad \text{for L3 profile}$$

$$y_w = \frac{b_f}{2} \quad \text{for T profile.}$$

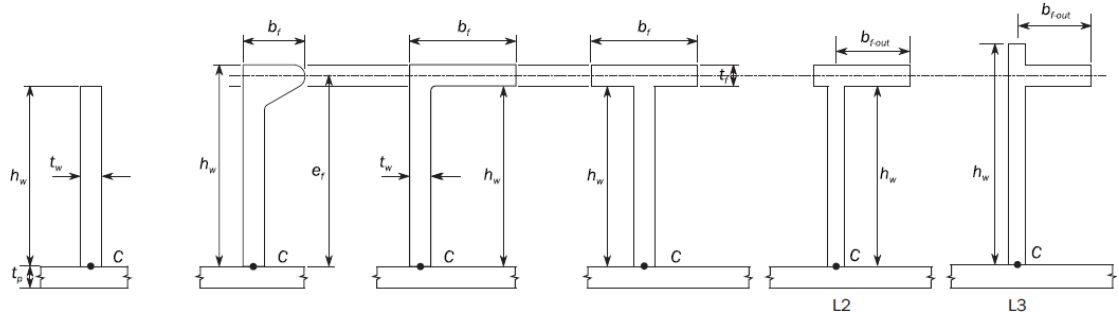


**FIG. 4.1**

Stiffener sections.

#### 4.2.2 Torsional buckling capacity

As it seems from the above warping stress formula, torsional buckling stress for the stiffened panel is contained among the components. A new assessment of torsional buckling for a stiffened panel,  $\sigma_{ET}$ , is suggested:

$$\sigma_{ET} = \frac{E}{I_P} \left\{ (I_w + I_z e_f^2) \left( \frac{m\pi}{\alpha} \right)^2 + \frac{1}{2(1+\nu)} I_T + \left( \frac{\alpha}{m\pi} \right)^2 \epsilon \right\} \quad (4.9)$$

where

$I_P$ : Net polar moment of inertia of the stiffener about point C, in  $mm^4$ .

$I_w$ : Net sectional moment of inertia of the stiffener about point C, in  $mm^6$ .

$I_T$ : Net St. Venant's moment of inertia of the stiffener, in  $mm^4$ .

$I_z$ : Mass moment of inertia about axis z of the stiffener, in  $mm^4$ .

	Flat bars	T profiles	Bulb, angle, L2 and L3
$I_z$	$\frac{h_w t_w^3}{12}$	$\frac{A_f b_f^2 + A_w t_w^2}{12}$	$\frac{A_f b_f^2 + A_w t_w^2}{3} - \frac{(A_f b_f + A_w t_w)^2}{4A_s}$
$I_P$	$\frac{h_w^3 t_w}{3}$	$A_f e_f^2 + \frac{A_f b_f^2}{12} + \frac{A_w h_w^2}{3}$	For angle $A_f e_f^2 + \frac{A_f b_f^2}{3} + \frac{A_w h_w^2}{3}$ For bulb $A_f e_f^2 + \frac{A_f b_f^2}{3} + \frac{A_w (h_w - t_f)^2}{3}$
$I_T$	$\frac{h_w t_w^3}{3}$		$\frac{A_f t_f^2}{3} + \frac{A_w t_w^2}{3}$
$I_w$	$\frac{h_w^3 t_w^3}{36}$	$\frac{A_f^3}{144} + \frac{A_w^3}{36}$	$\frac{A_f^3}{36} + \frac{A_w^3}{36}$

TABLE 4.1

Section properties for stiffener profiles

$e_f$ : Distance from attached plating to center (C) of flange, in  $mm$ , as shown in Fig. 4.1 to be taken as:

$e_f = h_w$  for flat bar profile.

$e_f = h_w + 0.5t_f$  for angle, L2 and T-profile.

$$\epsilon = \left( \frac{3b}{t_p^3} + \frac{2h_w}{t_w^3} \right)^{-1} \quad (4.10)$$

In the new equation, the effect of the attached plating on the model is introduced by adding the interaction of the plating with the stiffener through value  $\epsilon$ . It is evident that there is not a straightforward procedure for the evaluation of that interaction, and it is always a vexed issue to judge plate/stiffener interaction.

Of a great interest is to identify the relative contribution of each component of eq.(4.10) to the total torsional buckling capacity of the stiffened panel. In that event, eq.(4.10) has been discretized in four components.

$$\sigma_{ET} = \frac{E}{I_p} I_w \left( \frac{m\pi}{\alpha} \right)^2 + \frac{E}{I_p} I_z e_f^2 \left( \frac{m\pi}{\alpha} \right)^2 + \frac{1}{2(1+\nu)} I_T + \left( \frac{\alpha}{m\pi} \right)^2 \epsilon \quad (4.11)$$

$$\sigma_{ET} = \sigma_1 + \sigma_2 + \sigma_3 + \sigma_4 \quad (4.12)$$

For a more accurate interpretation of the above values it could be proper to examine the contribution of each component to the ultimate buckling capacity of the stiffened panel (Fig. 4.2).

Taking the case of a 0.25 m height flatbar of length,  $a = 3.2m$  and span,  $b = 0.7m$ , the first three terms present a smooth fluctuation as the number of half waves increases. Warping stresses (sum of  $\sigma_1$  and  $\sigma_2$ ) are close to zero for the first half waves and upsize while deformations increase. St. Venant's effect ( $\sigma_3$ ) introduces a significant value, constant and independent of the formed half waves on the model. On the other hand, the effect of the attached plating to the stiffener ( $\sigma_4$ ) predominates for small numbers of  $m$  but demonstrates a rapid fall as it moves to a higher range of half waves.

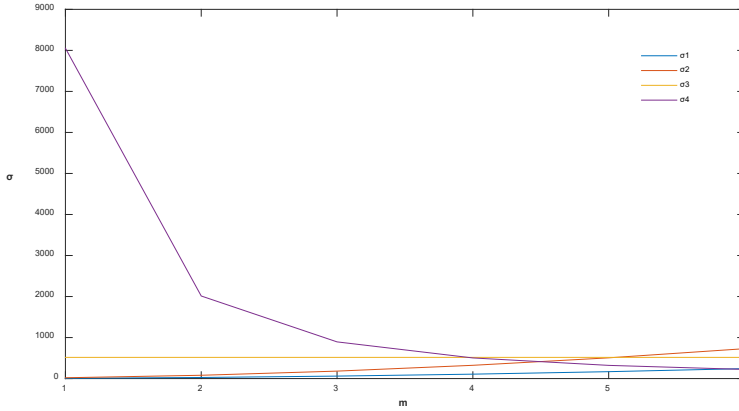


FIG. 4.2

Distribution of  $\sigma_1$ ,  $\sigma_2$ ,  $\sigma_3$  and  $\sigma_4$  in respect with the number of half waves,  $m$ , for flatbar.

However, for flatbars the expected number of halfwaves on the stiffener equals to the aspect ratio of the plating, due to the absence of the upper flange. Thus, for a flatbar having a stiffener buckling pattern of 4 to 5 halfwaves, as these from the previous chapter, all components feature relatively the same to ultimate torsional buckling capacity.

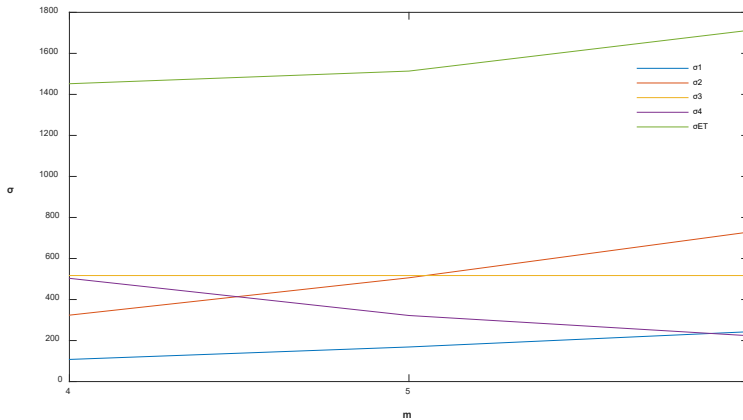


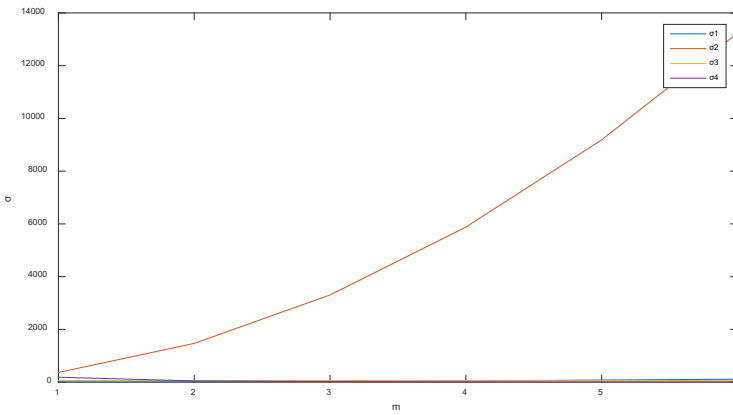
FIG. 4.3

Distribution of each component to ultimate torsional buckling capacity for 4 to 6 halfwaves, for flatbar

The aforementioned results correspond to stiffeners with no flange at the top. Repeating the procedure for stiffeners containing flange, could highlight the contribution of the flange in buckling capacity of the stiffeners towards torsion.

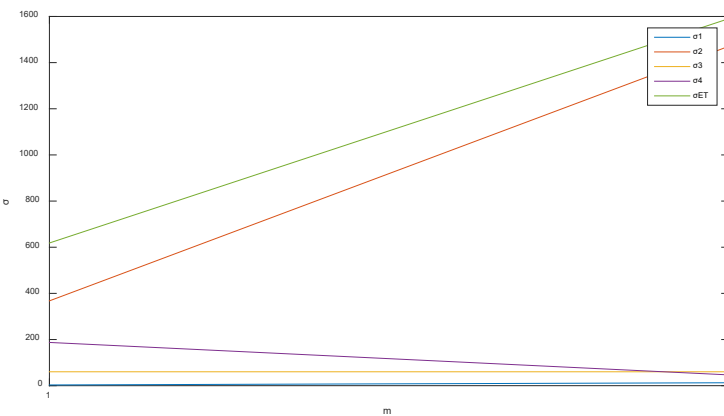
Specifying a common 0.6m height T-stiffener of length,  $a = 3.2m$  and span,  $b = 0.7m$ , its behavior alters significantly compared to flatbars. The second component dominates over the

rest for increasing halfwaves, following an exponential path, which indicates that  $e_f$ , the distance of the attached plating to the center of the flange, is what determines eventually the resulting capacity of the stiffener in torsion. Therefore, the existence of the upper flange changes the present stresses each part offers.


**FIG. 4.4**

Distribution of  $\sigma_1$ ,  $\sigma_2$ ,  $\sigma_3$  and  $\sigma_4$  in respect with the number of half waves,  $m$ , for T-stiffeners.

In this case, webs of T-stiffeners are bound by the flange, thus are prompt to buckle in one half wave. For that values,  $\sigma_2$  is still higher than the others and the effect of the attached plating is defining the result as well. However, a comparison of ultimate torsional buckling capacity of the two sections emphasizes that flatbars demonstrate significant resistance against torsion, attaining higher values of torsional buckling capacity.


**FIG. 4.5**

Distribution of each component to ultimate torsional buckling capacity for one halfwave, for T-stiffener



## 5. Results from Assessment Methods

### 5.1 General

In the most marine structures the majority of stiffeners attached on plate panels are flatbars, T or L profiles. Undoubtedly, the final response of the structure and, by extension, its ultimate buckling capacity is highly impacted by the selected stiffener and its interaction with the plating. Therefore, a detailed analysis of the aforementioned parameters is inevitable, in order to choose appropriately the correct stiffener type that corresponds to the potentially induced loads.

In the following paragraphs, a complete finite element analysis of different stiffeners of varying dimensions, under a wide range of loadings is held. First, a linear analysis will demonstrate the elastic buckling behavior of each model, presenting their emerging buckling modes. Then, the appropriate buckling “shapes” will be introduced in nonlinear analysis, in order to evaluate the effect of initial imperfections and alternating loadings in ultimate buckling capacity.

### 5.2 Panels with Attached T-stiffeners

T-stiffeners are more frequently used in construction among the other stiffener types, due to their geometry. Considering the section of the plate (effective width of the plate) and the attached stiffener as an I section of a beam, the web resists shear forces that are transferred from the plate, while the flanges resist most of the bending moment experienced by the beam.

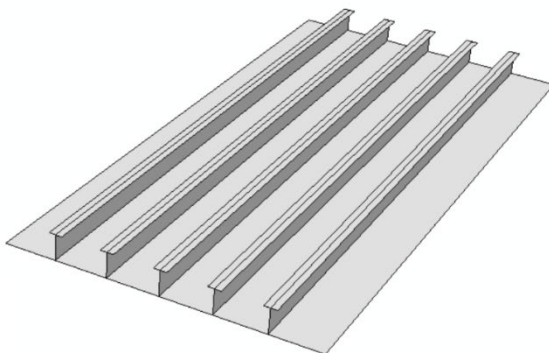


**FIG. 5.1**

Longitudinally stiffened panel with T-section stiffeners

Beam theory shows that the I-shaped section is a very efficient form for carrying both bending and shear loads in the plane of the web. On the other hand, the cross-section has a reduced capacity in the transverse direction, and is also inefficient in carrying torsion.

T-stiffeners with different geometrical dimensions were chosen during the FEA. A wide range of web heights and thicknesses has been modeled, so that torsional buckling could be feasible. Although the proposed geometrical dimensions describe a generally stiff panel, modifications on web geometry contribute enough on its torsional flexibility.

Type	L	s	<b>h<sub>w</sub></b>	<b>b<sub>f</sub></b>	<b>t<sub>p</sub></b>	<b>t<sub>w</sub></b>	<b>t<sub>f</sub></b>
Panel400	3200	800	400	200	22	12	22
Panel450	3200	800	450	200	22	20	22
Panel500	3200	800	500	200	22	20	22
Panel550	3200	800	550	200	22	20	22
Panel600	3200	800	600	200	22	20	22
Panel650	3200	800	650	200	22	20	22
Panel700	3200	800	700	200	22	20	22
Panel750	3200	800	750	200	22	20	22
Panel800	3200	800	800	200	22	20	22
Panel850	3200	800	850	200	22	20	22
Panel900	3200	800	900	200	22	20	22
Panel950	3200	800	950	200	22	20	22
Panel1000	3200	800	1000	200	22	20	22
Panel1050	3200	800	1050	200	22	20	22
Panel1100	3200	800	1100	200	22	20	22

TABLE 5.1

T-section dimensions

Below, some of the panels will be examined in full detail, aiming to the assessment of different load cases on their buckling capacity and ultimate strength. During the analysis, plate and flange widths are equal, while web height and width change gradually.

The aspect ratio of the plate is  $a = \frac{3200}{800} = 4$ , thus during eigenvalue analysis, modes forming four half waves between transverse girders at plate plane describe accurately local buckling failure. On the other hand, stiffeners are considered as beam-columns and for this reason are expected to buckle in one half wave.

During nonlinear analysis, tolerance levels corresponding to the maximum displacements that the plate and the stiffeners could take are 4mm and 3.2mm respectively.

### 5.2.1 Panel T-400

Panel 400 is a stiffened panel with the smallest proposed stiffener height. Generally, a stiffener with a web height of 400mm and stiffener span of 800mm is considered as moderate-height stiffener.

### Linear Analysis

When the short edge of the model is subjected to pure axial compression, the first arising eigenmodes establish local plate buckling over torsional buckling, as the dominant failure mode. Although a 15 mm thickness of the stiffeners is relatively small value, the 22 mm flange width maintains a high bending resistance of the stiffener.

Even though the first eigenmode shows a localized effect of local plate buckling on the edges, the critical part of the model is considered in the middle. There, four half waves are being formed and pure plate buckling conditions are approached at a high level. A slight torsion of the stiffeners at the edges could be regarded negligible. Torsional buckling develops several eigenmodes later (eigenmode 33). Exceeding enough the critical load could lead to reduced rotational flexibility of the web, inducing the stiffeners to buckle in one half wave in longitudinal direction, but with limited deformations of the plate.

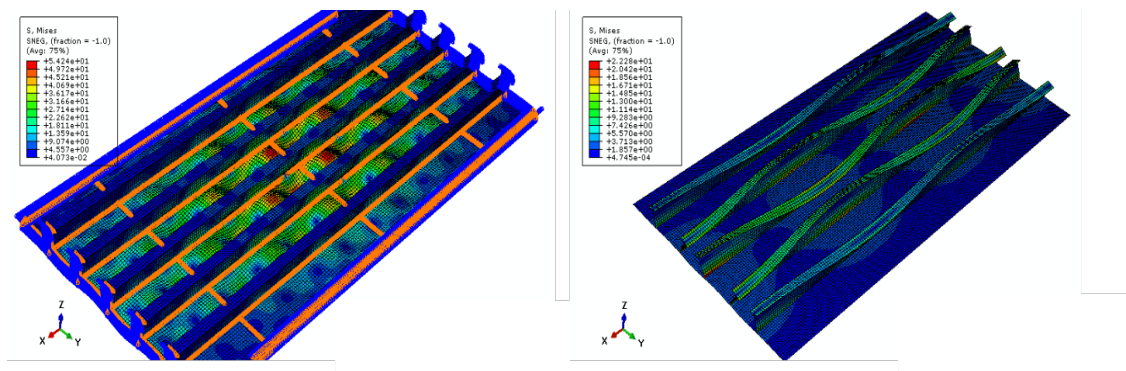


**FIG. 5.2**

Eigenmodes for pure axial compression (1-plate, 33-stiffener)

In order to assess the influence of geometrical dimensions on the torsional flexibility of the stiffeners, an attempt to remodel the stiffeners with 10mm web and 16mm flange thickness had been made. The goal was to reduce the moment of inertia of the stiffener by limiting the contribution of the flange and the web in it, so that it could be easier to bend. Even though the thickness of the flange was significantly reduced, eigenmodes still establish strong stiffeners towards torsion, formulating at the 20<sup>th</sup> eigenmode the first torsional buckling mode. Additionally, the plate itself provides great support to the web, preventing it from torsion, unless high loading conditions are reached.

A careful reevaluation of the width of the flange in accordance to its flexural resistance could result to torsional buckling of the stiffeners, but this is something that consumes time and does not serve the goals of that project.

On the next step, a transverse compressive stress will be added in the longitudinal edge, equal to 20% and 40% of the axial one.

A 20% transverse load maintains plate buckling as the dominant failure mode, while torsional buckling of the stiffeners appears earlier than before, on the 22<sup>nd</sup> eigenmode, but they still remain strong under bending. It seems that the presence of moderate transverse stresses does not significantly affect stiffeners.

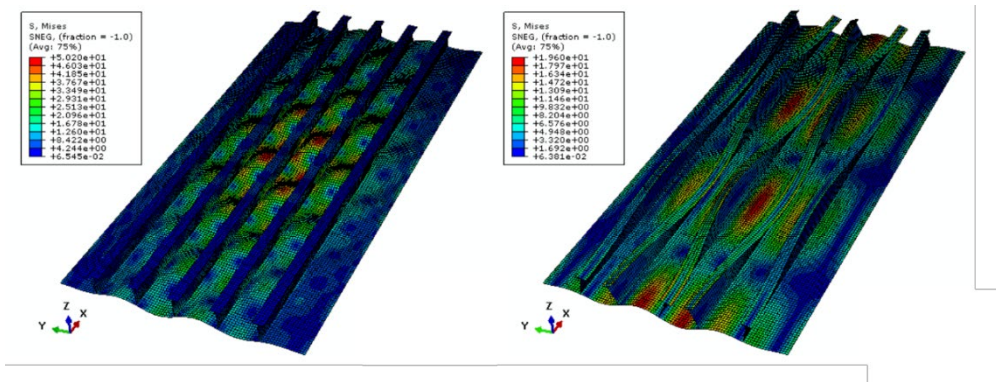


**FIG. 5.3**

Eigenmodes for 20% biaxial compression (1-plate, 22-stiffener)

Increasing the transverse load to 40% overturns the sequence of the appeared eigenmodes. Stiffeners rotate before local plate buckling occurs, a fact that highlights that a higher transverse load strengthens the capacity of the plate itself, but reduces bending resistance of the stiffeners, inducing the structure to collapse.

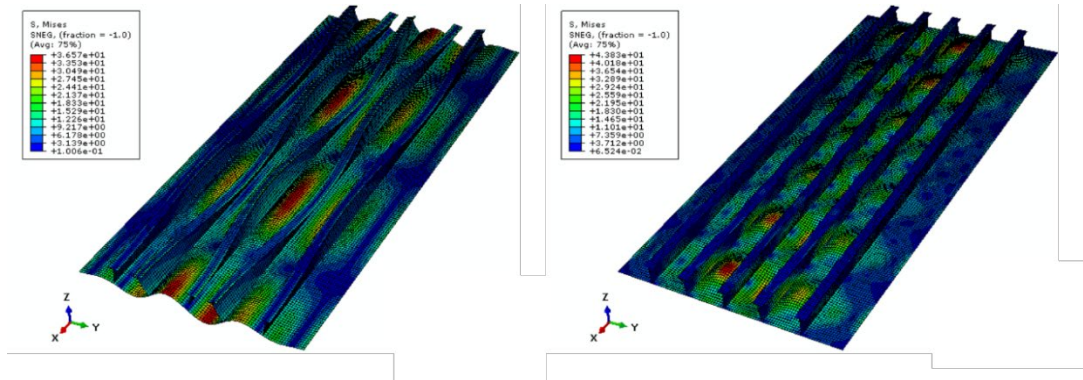


**FIG. 5.4**

Eigenmodes for 40% biaxial compression (2-stiffener, 11-plate)

A distributed pressure acting at the bottom of the model will be added. Lateral pressure magnifies plate's curvature. The bottom plate attains a sinusoidal shape, illustrating flexural deformation.

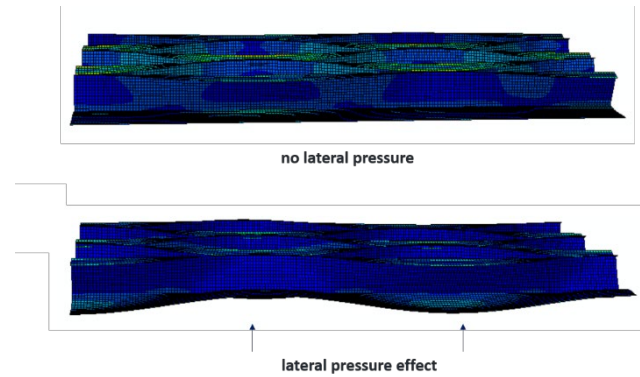


**FIG. 5.5**

Effect of lateral pressure at the bottom surface of the model

The way lateral pressure is introduced in the analysis influences ultimate buckling capacity. There are two approaches to simulate lateral pressure. The first assumes that lateral pressure increases proportionally similar to in-plane loads. In the other, lateral pressure is regarded constant, set as a “dead load” before eigenvalue analysis. Therefore, only in-plane loads increase proportionally. Both ways are examined, in order to evaluate their impact on ultimate buckling capacity of the stiffened panel.

Constant pressure at the bottom of the panel attains an initial stress condition. Before linear analysis, the shape of the plate between stiffeners and transverse girders, as well as stiffeners, are deformed. When analysis begins, the axial and transverse increasing stresses are superimposed to an already imperfect shape. On the contrary, when both pressure and in-plane loads begin to act simultaneously, the analysis starts with a perfectly shaped model.

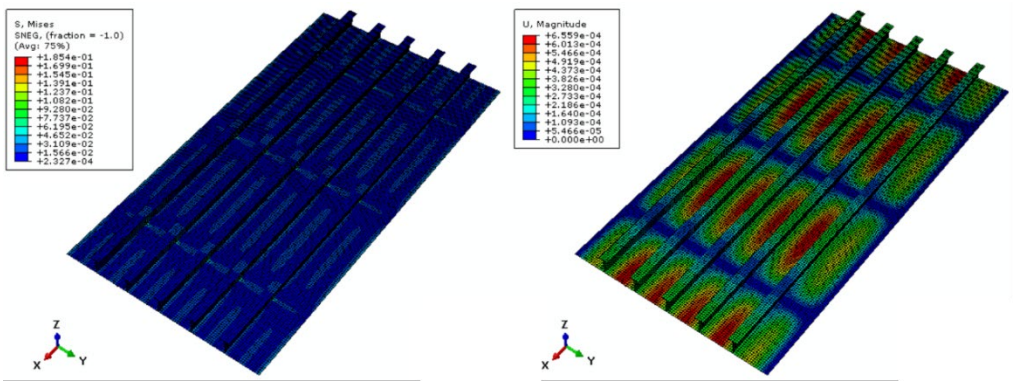


**FIG. 5.6**

Von Mises stresses and mean deformations for lateral pressure set as a preload

Both approaches amplify the effect of torsion on the stiffeners, even though the value of lateral pressure is regarded small. Proportional increase of the lateral pressure is devastating for the structure, as it forces stiffeners to rotate immediately. On the contrary, setting it as a preload leads the plate to receive major deformations while reaching the bifurcation load. In this case, stiffeners are quite stronger and flange contributes in keeping a stable state. However, stresses that provoke torsional buckling are close to critical, so the structure is still at risk of collapse.

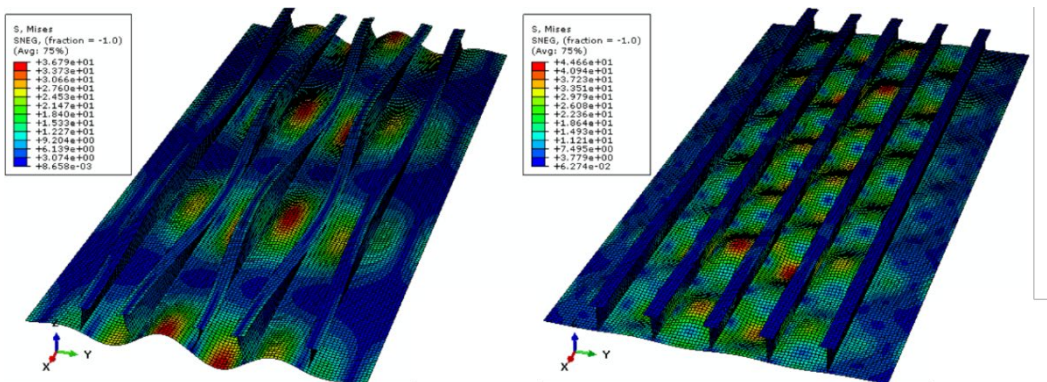


**FIG. 5.7**

Eigenmodes for 40% transverse loading and increasing lateral pressure (1-stiffener, 11-plate)

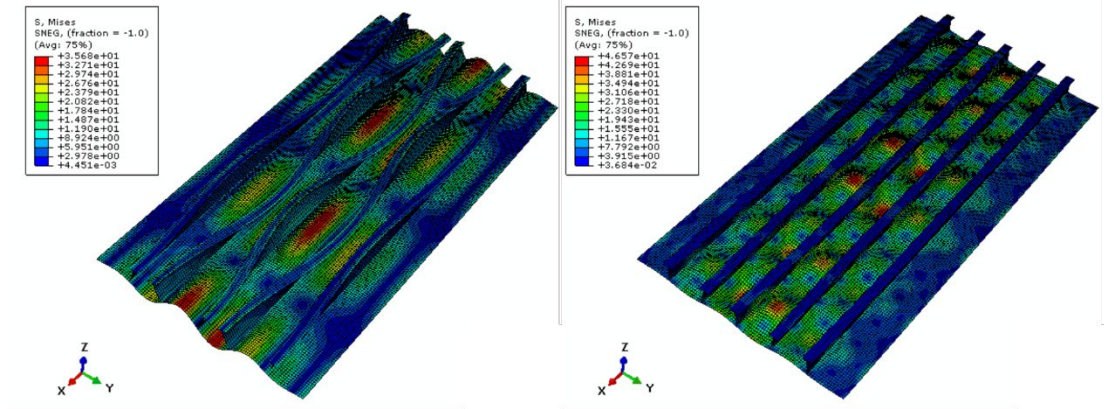


**FIG. 5.8**

Eigenmodes for 40% transverse loading and lateral pressure as a preload (4-stiffener, 12-plate)

Calculation of the elastic (critical) buckling stresses for each loading case (Table 5.2) highlights a remarkable reduction of structure's capacity, while loading conditions become more complex. Pure axial loads demand greater magnitudes to cause deformations on the model, whereas biaxial stresses weaken it faster. When they are combined with lateral pressure too, the structure is prompt to buckle under even lower stress levels. Comparing the two approaches of lateral pressure, the difference is not on the magnitude of the demanded stresses that will buckle the model, but mostly on the sequence failure modes appear.

The eigenmodes below represent the modes where pure versions of torsional buckling of stiffeners and local plate buckling appear. The eigenvalues are factorized and have no physical substance, therefore the corresponding elastic stresses are derived in respect to plate thickness. During nonlinear analysis these selected eigenmodes would describe the initial geometrical imperfections of the plate and the stiffener.

It is observed that the arising elastic stresses of lateral pressure illustrate negligible differences for both cases. This proves that for that web height, at the time of buckling constant pressure is very close to the increasing pressure levels, thus the way lateral pressure is applied does not affect the resulting critical stresses.

	Eigenmode	Eigenvalue	FEA elastic buckling stress (MPa)
pure axial compression	1 (plate)	13849	630
	33 (stiffener)	18413	837
20% stress ratio	1 (plate)	11371	517
	22 (stiffener)	14389	654
40% stress ratio	2 (stiffener)	9010	410
	11 (plate)	10014	455
increasing pressure	1 (stiffener)	8568	389
	11 (plate)	9930	451
constant pressure	4 (stiffener)	8721	396
	12 (plate)	9669	440

TABLE 5.2

Elastic buckling stresses for each loading case of T-400

### Nonlinear Analysis

The aforementioned eigenmodes would be utilized as initial geometrical imperfections of plate/stiffeners, applied with the proposed tolerance levels. The first eigenvalue will be used as the applied load, proportionally increased until reaching its maximum value.

During the analysis, the characteristic curve of load proportionality factor reaches its peak on an almost linear trend and drops quickly after bifurcation load.

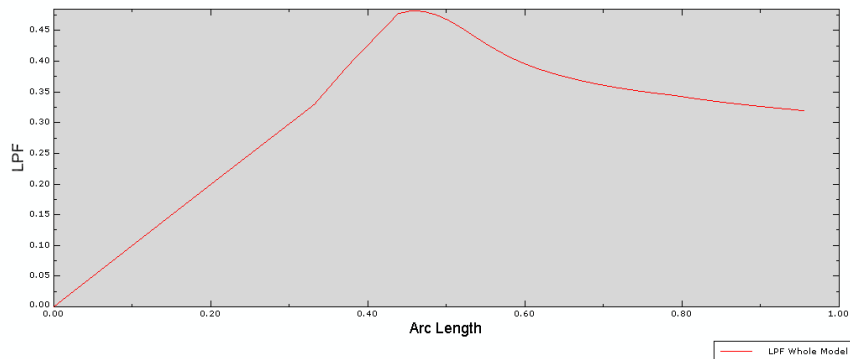


FIG. 5.9

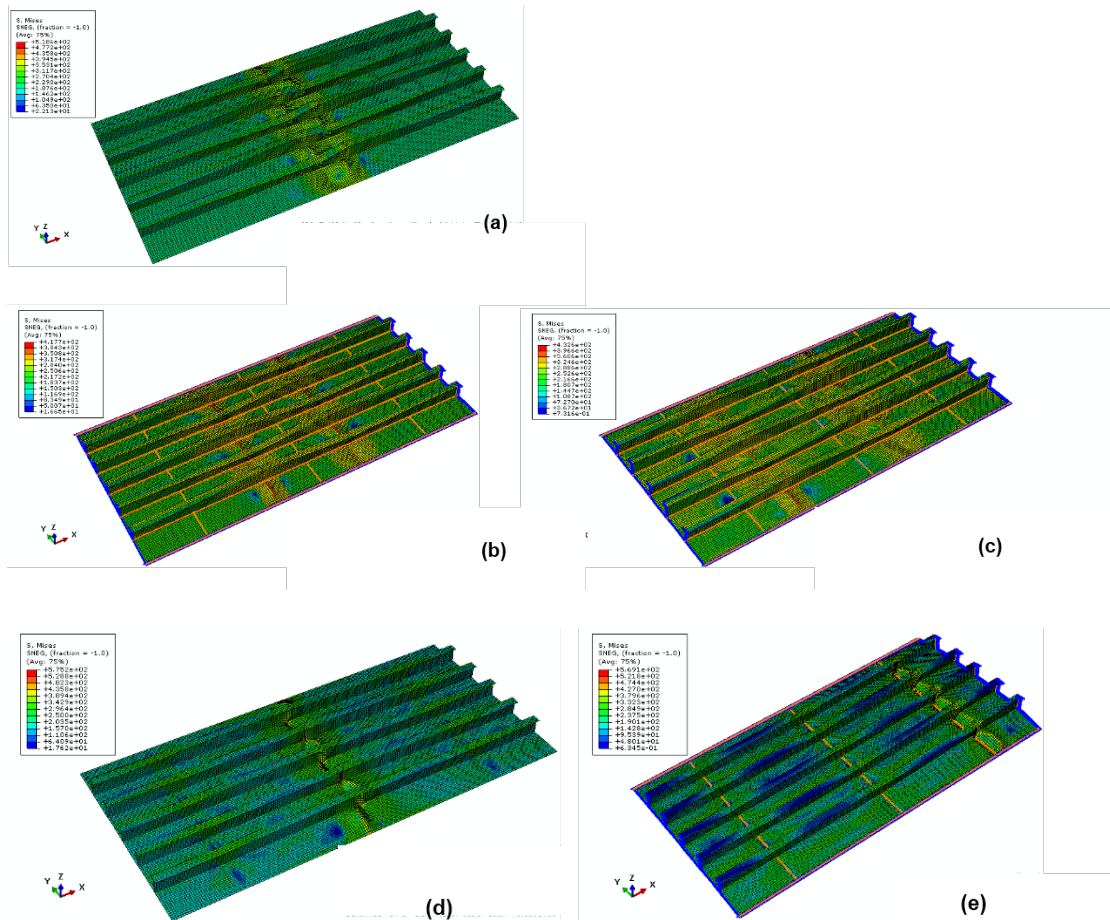
Load proportionality factor curve

After exceeding critical buckling load, each model yields both at the plate and the stiffeners. Always, torsion of the stiffeners is accompanied by plate deformations, mainly induced due to

the constraint interaction between them. Depending on the loading case, each model's failure localizes at different parts.

Starting with the act of axial compression of the short edge, the stresses concentrate in the middle girder, where stiffeners loose their torsional durability and collapse. As transverse compression is added, yielding tends to delocalize forming two separate failure parts instead of one, that seem to translate away from the middle girder of the panel, while transverse loads increase. Simultaneously, their distance becomes wider with ascending values of loads. At this place, stiffeners are susceptible to torsional buckling, possibly amplified by local plate buckling too.

The effect of lateral pressure reestablishes the failure at one region, but on different places, depending on the way pressure is applied. The plate buckles locally and transfers shearing forces to the webs, forcing them to rotate. Considering that lateral pressure increases proportionally results in overturning of the stiffeners close to the middle girder. When is regarded as an already existing load, the stiffened panel buckles first close to the last girder.


**FIG. 5.10**

Von Misses stresses for (a) pure axial, (b) 20% biaxial, (c) 40% biaxial compression, (d) increasing lateral and (e) constant lateral pressure

Maximum deformations at the top flange and the plate follow a switching of tension/compression, at the same region that maximum stresses dominate. Maximum displacements in transverse direction, U2, illustrate deformations of the top flange, whereas in vertical direction, U3, deformations of the plate. Each loading version corresponds to similar motif of deformations.

The only difference in deformation distribution comes when lateral pressure is a preload. In this case, although stiffeners bend, maximum deformations are observed in plate area close to the unloaded short edge, forcing it to move upwards.

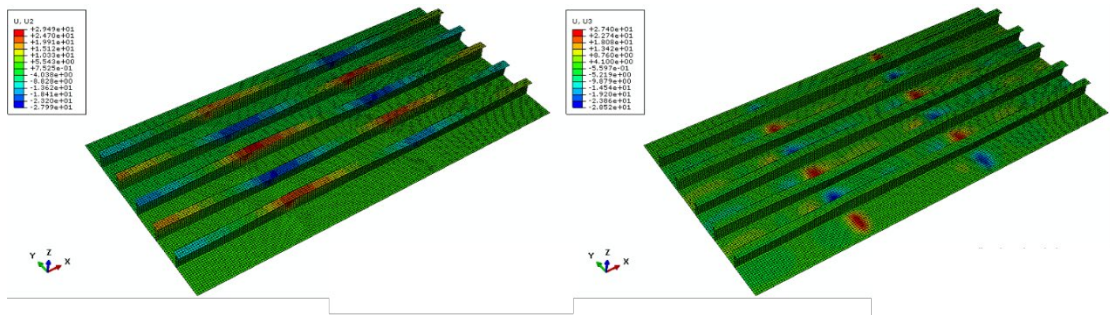


**FIG. 5.11**

Maximum deformations, U2 and U3, at y and z axis (for 40% biaxial compression)

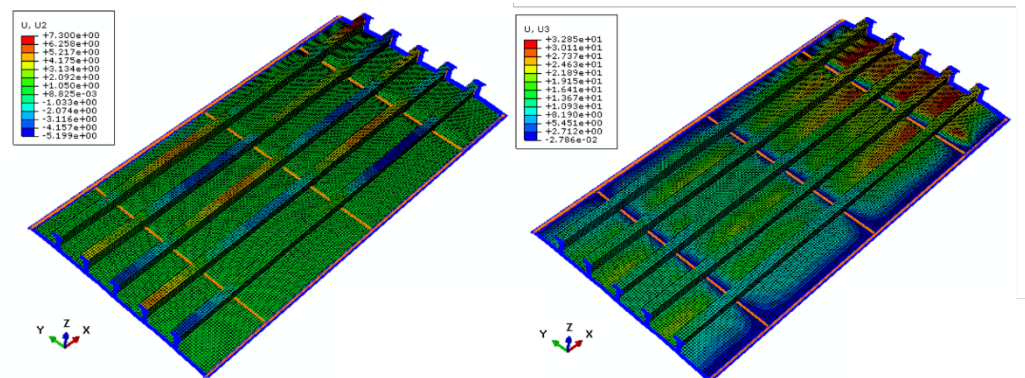


**FIG. 5.12**

Maximum deformations, U2 and U3, at y and z axis (for 40% lateral pressure as a preload)

Lateral pressure application seems to define the ultimate capacity of the structure. Both approaches estimate maximum stresses enough below yielding stress, thus buckling anticipates material yielding. A proportional increase of lateral pressure attains the highest capacity levels compared, explaining that including lateral pressure on Riks method

overestimates the ultimate strength of the structure. On the other hand, constant pressure approaches reality conditions and leads to a more conservative evaluation of ultimate stresses.

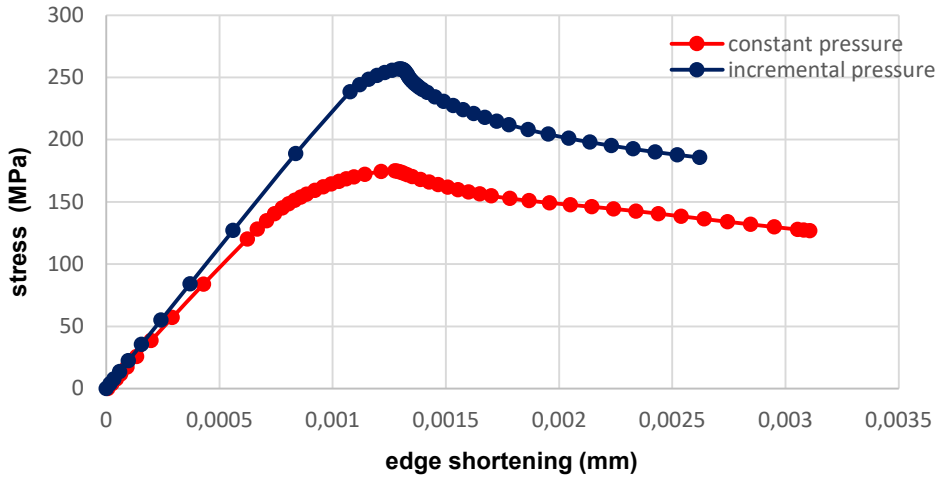


**FIG. 5.13**

Effect of different applications of lateral pressure on ultimate capacity evaluation

### Ultimate Buckling Capacity of Panel T-400

Results of eigenvalue analysis, conclude that pure axial compression and/or low biaxial effects, lead the structure to maintain high resistance to stiffener's bending and is not expected to collapse before material yielding. On the contrary, under increased biaxial loading or lateral pressure, stiffener's strength is not sufficient to withstand the induced stresses and they are suspected to overturn, directing the whole structure to collapse.

After appropriate calculations, shortening of the loaded edges, as well as ultimate capacity of the stiffened panel, are estimated in high accuracy.

Each of the curves represent the results of nonlinear FEA for cases A, B, C. The vertical axis describes the resultant stress level the structure could anticipate, in MPa, while the horizontal axis shows the displacement of the transverse loaded edge, in mm. Material yielding occurs at 315 MPa, a value over which none of the curves exceed, thus buckling develops prior to yielding failure. Every curve is distinguished in two parts; the elastic, where the curve varies linearly with load and the inelastic, after the bifurcation point. The bifurcation point is the maximum of each curve and represents the ultimate buckling capacity of each model. The structure is considered to lose its stability after reaching its ultimate buckling capacity.

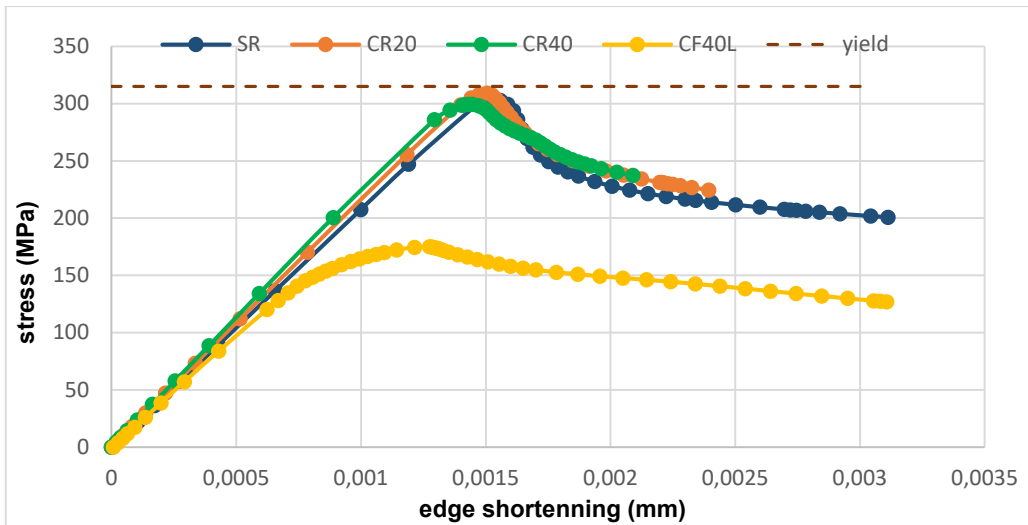


FIG. 5.14

Ultimate buckling capacity of T-400 panel

It seems that all cases, except from this of lateral pressure, display approaching peak values of the von Misses stresses. Especially pure axial and biaxial compression of 20% present identical behavior, having critical stresses close to yielding. Higher transverse loads translate the curve a bit lower, yet not notably, with a critical buckling stress of roughly 300 MPa. In addition, axial and moderate compression result to a maximum edge shortening is around 0.0015mm, whereas with lateral pressure the shortening falls to 0.012mm before instability occurs. This remarks that under low edge stress ratios the buckling capacity of the structure gets hardly effected.

A great drop in buckling capacity to almost the half happens when pressure is applied at the bottom of the model. The curve corresponds to lateral pressure set as a preload, which is the most unfavorable case. The maximum stresses are close to 175 MPa and maximum deformations before buckling initiate quicker than in the rest cases.

### 5.2.2 Panel T-600

Increasing the height of the web to 600 mm and its thickness to 20 mm and keeping the rest of the variables constant, Panel 600 will be examined for all loading cases.

#### Linear Analysis

Stiffeners of 600mm height cannot withstand pure axial compression without enduring torsion immediately. Stiffeners rotate around x-axis in one half wave between each transverse girder. Plate buckling failure appears after a slight increase of the critical load. Both eigenmodes illustrate the corresponding failures on a pure version, which means that plate/stiffener buckling modes get not mixed up. In plate's failure mode, although at the surface of the web local buckling appears, it is mainly induced from interaction with the plate.

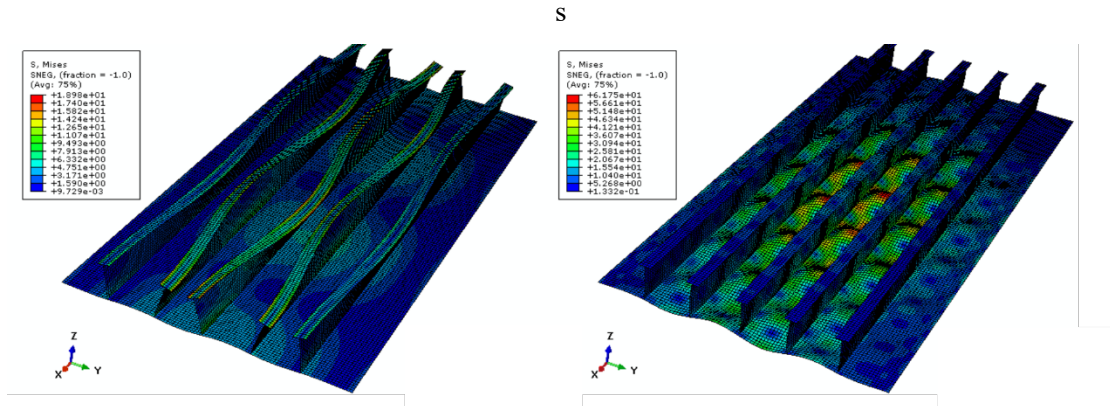


**FIG. 5.15**

Eigenmodes for pure axial compression (1-stiffener, 4-plate)

Adding in-plane loads in transverse direction with a gradual increase of 10%, 20% and 40%, as well as lateral compression, results to quite similar conditions to pure axial compression. Stiffeners are proved to be weaker than the plate, thus torsional buckling predominates in all cases. The developed buckling shapes show insignificant differences between them and there is no necessity to present them in detail.

A decline of the typical shapes is made when lateral pressure as a preload is applied. While the edges of the panel were almost straight, now they are being “pushed” by the bottom distributed load and curvature between each transverse and longitudinal stiffener gets magnified.

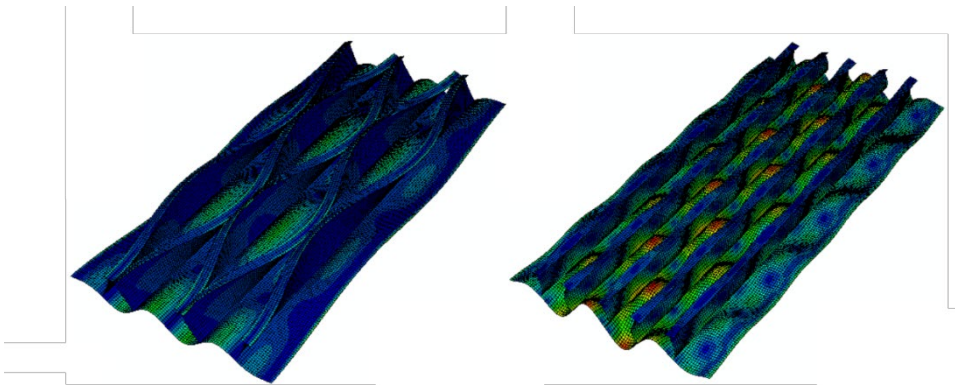


**FIG. 5.16**

Effect of constant lateral pressure on panel's curvature.

Referring to the arising buckling modes, the stiffeners of the panel are most contingent to be subjected to torsional buckling after the critical buckling load has been reached. The different loading conditions seem not to effect the sequence of the emerging eigenmodes or the cause of failure. However, torsional buckling mode appears almost purely, containing some local plate buckling, mainly induced from their own rotation about their long dimension. In the same way, the modes representing local plate buckling include a slight deformation of the web's surface as well.

Apparently, combined loadings constitute a more severe danger for the structure. As the transverse loads increase the stiffened panel displays lower potential to withstand forces without buckling. Especially when highly transverse loads are applied, the capacity of the structure falls rapidly and buckling occurs faster. Lateral pressure, independently of the path that is used, decreases the elastic buckling capacity of the stiffened panel. Yet, considering lateral pressure as a dead load attains slightly higher levels of elastic capacity. Torsional buckling of the stiffeners is still the most possible collapse mode.

Calculation of the corresponding eigenvalues from FEA provides the elastic buckling capacity for each given failure mode.

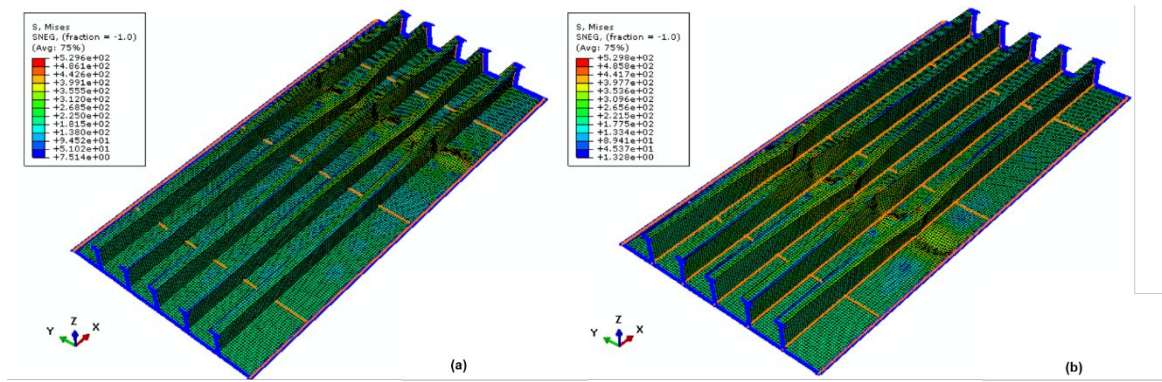
	Eigenmode	Eigenvalue	FEA elastic buckling stress (MPa)
pure axial compression	1 (stiffener)	13460	612
	4 (plate)	14758	671
10% stress ratio	1 (stiffener)	12482	567
	4 (plate)	13361	607
20% stress ratio	1 (stiffener)	11652	530
	2 (plate)	12333	561
40% stress ratio	1 (stiffener)	8847	402
	3 (plate)	10083	458
increasing pressure	1 (stiffener)	8286	377
	18 (plate)	11102	505
constant pressure	1 (stiffener)	8536	388
	4 (plate)	9994	454

**TABLE 5.3**

Elastic buckling stresses for each loading case of T-600

### Nonlinear Analysis

For each nonlinear analysis, the position of the failure differs but occurs in an area between the girder span. At that part stiffeners lose their rotational resistance and warp, leading to collapse of the web and local plate deformations as well. Maximum displacements show that after buckling, a combined yielding of the plate and the stiffener emerges where maximum stresses concentrate. Again, along the failure surface a switch of tension/compression is developed.


**FIG. 5.17**

Von Misses stresses for (a) 20% biaxial and (c) 40% biaxial compression

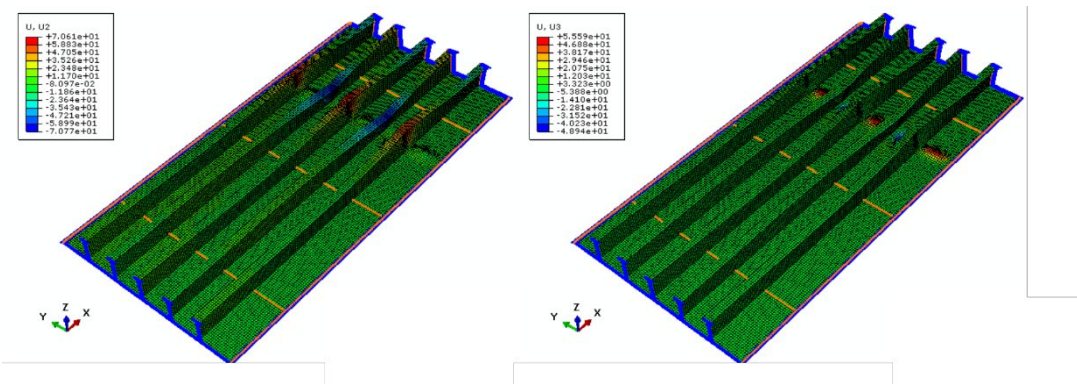


**FIG. 5.18**

Maximum deformations, U2 and U3, at y and z axis (for 20% biaxial compression)

The only difference comes when lateral pressure increases proportionally. At that time, the intersection of the back transverse girder and stiffeners becomes weak and cannot carry the induced loads, leading to their overall collapse until reaching the unloaded short edge.

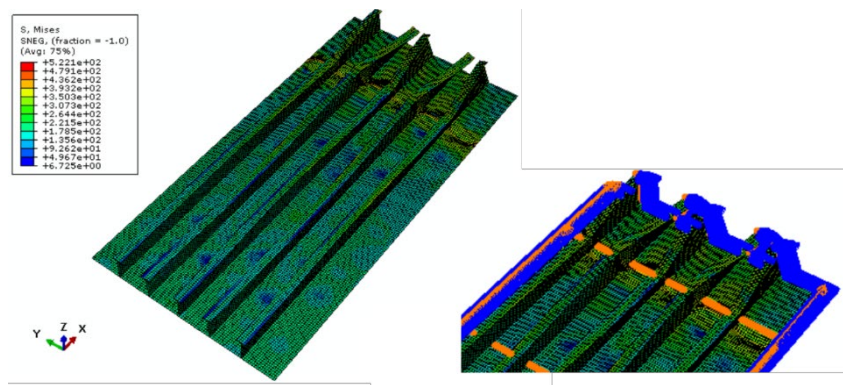


**FIG. 5.19**

Von Misses stresses for increasing lateral pressure

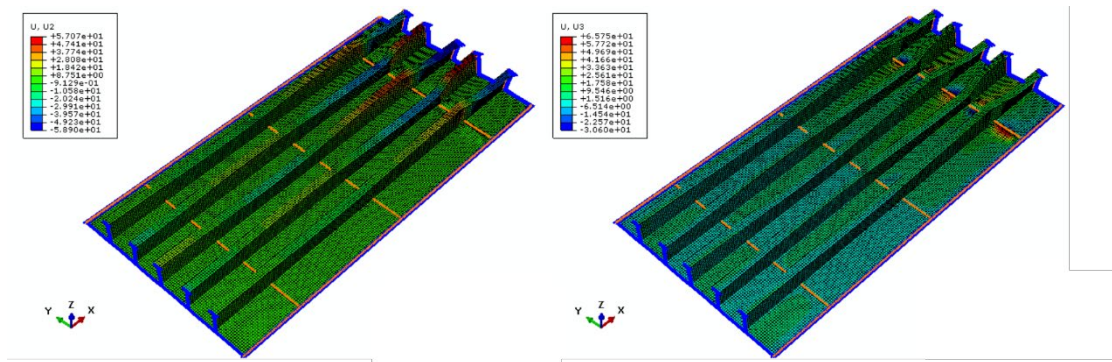


**FIG. 5.20**

Maximum deformations, U2 and U3, at y and z axis (for increased lateral pressure)

Once again, lateral pressure effects differently the performance of the model depending on the way it is applied. The stress/strain curves coincide during the elastic range, but bifurcation load is reached quicker for increasing pressure. The maximum structure's capacity is 300 MPa, when preloaded pressure is considered, while the other case estimates no more than 279 MPa. These magnitudes are relatively close but lead to significant differences in terms of design load definition.

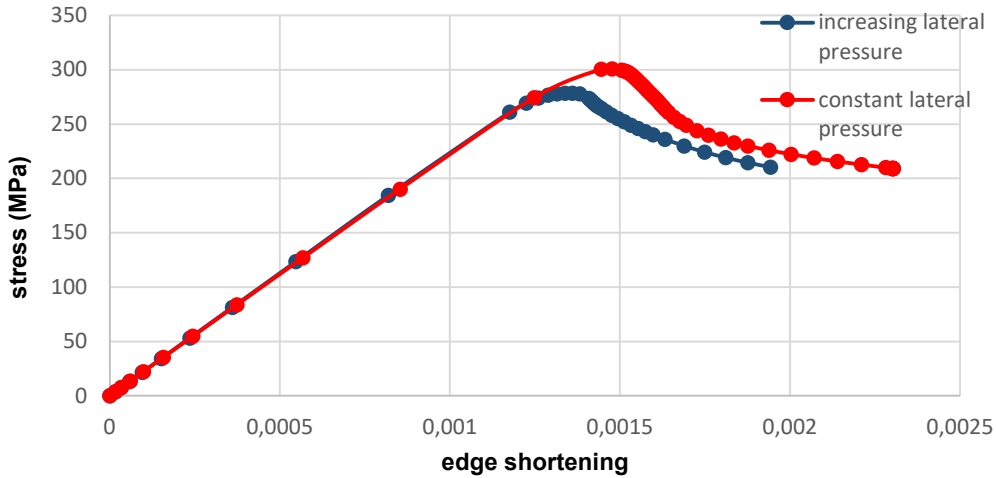


FIG. 5.21

Effect of lateral pressure on ultimate buckling capacity of T-600 panel

### Ultimate Buckling Capacity of Panel T-600

Results from linear analysis denote torsional buckling of the stiffeners as the major failure mode of the model. However, the stresses that could cause plate local buckling are close to critical, so that material yielding will evolve rapidly.

The following curves confirm that. Fig.5.22 represents the capacity curves from nonlinear FEA for loading cases A, B, C. Although lateral pressure as a preload is not the conservative one, it describes on a more accurate way real conditions.

Again, vertical axis illustrates the ultimate buckling capacity of the stiffened panel, in MPa, and horizontal axis shows the displacements of the transverse loaded edge, in mm. Pure axial compression maintains a high capacity level, close to 300 MPa, which is reinforced even more when modest transverse loads feature. In general, buckling failure occurs before yielding, although low magnitudes of biaxial loads tend to make uncertain whether the model would collapse due to buckling or yielding.

What is of great importance is the application of higher transverse loads on the model. It is proved that it is not able to withstand such loadings without losing a significant part of its capacity, thus it is subjected to collapse prior to the other cases. It is also interesting that equal magnitudes combined to lateral pressure increase model's capacity, moving the curve on the same level to pure axial compression.

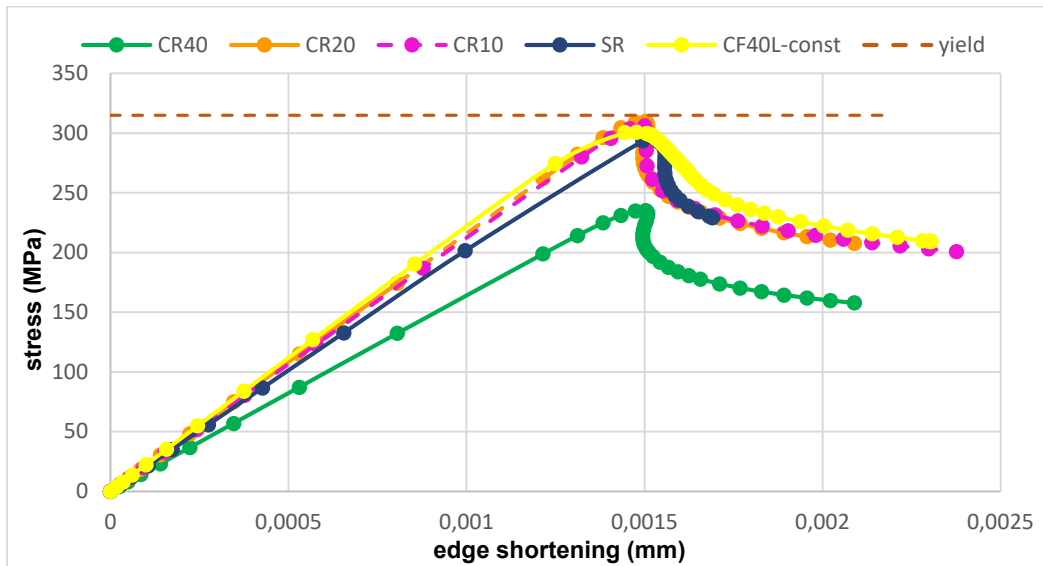


**FIG. 5.22**

Ultimate buckling capacity of panel T-600

### 5.2.3 Panel T-900

T-stiffeners with a web height equal to 900 mm are not very common in typical ship or offshore structures, as their geometrical dimensions are big enough and such webs are considered more like plates. Nonetheless, there are examples such as found in extreme tall L-type stiffeners in the actual design which are used under upper deck in VLCC (Very Large Crude Carriers), so it would be useful to assess their behavior under various loads.

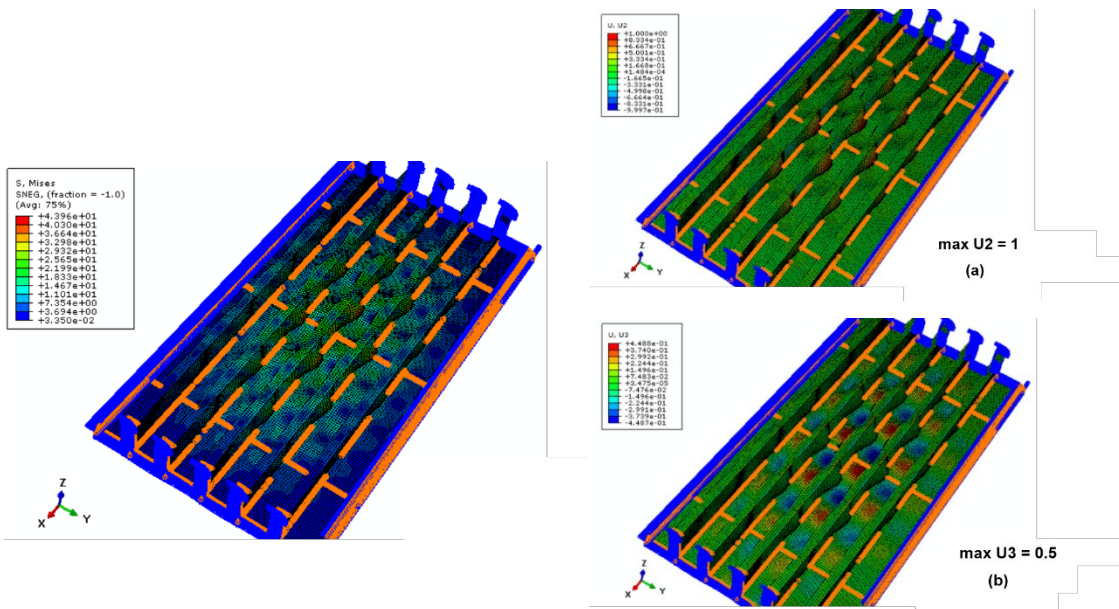
High web heights force shearing forces on the flange to elaborate greater magnitudes of torque, so it is suspected that failure of the stiffeners would predominate. The failure would be a mix of torsional and local in-plane buckling. Plate may not deflect immediately and main deformations could be caused due to the constraint that stiffeners provide on it.

## Linear Analysis

Applying axial compressive stresses results to completely different buckling formulations from what has been encountered previously. Looking through the results of linear analysis, torsional buckling of the stiffeners is developed at the initial collapse modes, constituting it the dominant source of failure. The flanges buckle by rotating about the x-axis, but maintain straight planes on the other two axes. That buckling pattern was expected, due to the increased height of the web and the narrow span between the stiffeners.

As for local plate buckling, a pure failure mode cannot be easily distinguished without including deformations at the surface of the web too. A wide range of eigenmodes with a mixture of plate and stiffener local buckling were available, making it hard to find the appropriate describing solely initial imperfections of the plate. This assessment process is always complex and is based on the subjective interpretation of the contextual engineer.

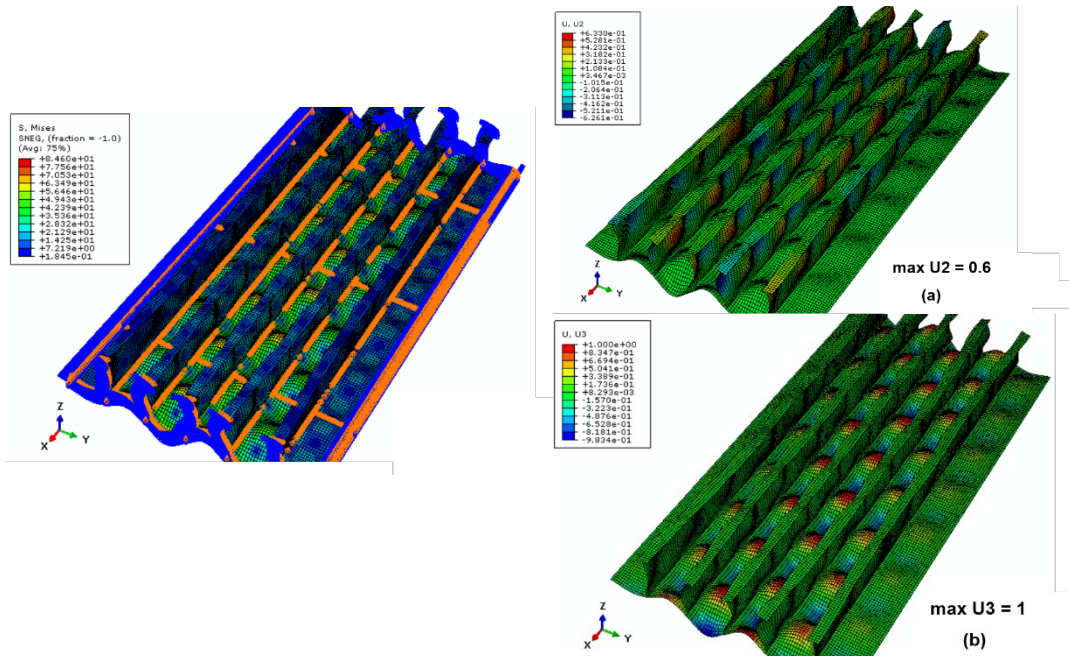
The first eigenmode after consequent torsional buckling modes that could describe local plate buckling (Fig. 5.23) will be examined in detail. Von Misses stresses concentrate their maximum values along web and plate surfaces. On both parts, four to five halfwaves are formed, agreeing with the aspect ratio of the plate. Furthermore, separate assessment of the maximum displacements, U2 and U3 that web and plate could receive in y and z directions respectively (fig. , a-b), prove that the factorized maximums for the web are double compared to the plate, so stiffeners are more effected from the interaction with the plate.



**FIG. 5.23**

Von Misses stresses and maximum displacements in y and z axis for plate local buckling failure (eigenmode 6)

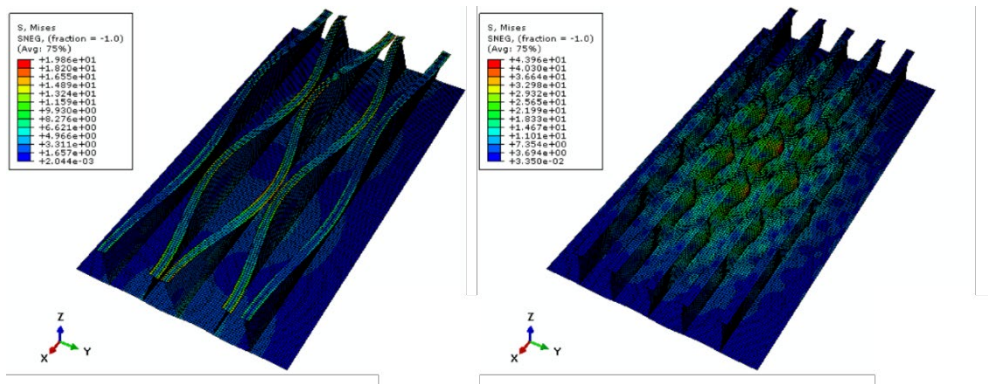
Further down, another sufficient failure mode is found, where high stress levels dominate in the plate compared to the web. Additionally, stiffeners rotate close to short edges, disturbing straight conditions but maintaining symmetry. Again, the arising number of half waves in both parts is satisfactory. Unlike the previous case, displacements U2 and U3 do not overestimate web's deformations but show maximum deformations on the plate.



**FIG. 5.24**

Von Misses stresses and maximum displacements in y and z axis for plate local buckling failure (eigenmode 97)

That is a typical example where both collapse modes fulfill quite sufficiently initial imperfections. On eigenmode 6, deformations on the stiffener are magnified so it is a more conservative approach, however it is closer to the minimum critical magnitude that could initiate buckling. On the other hand, eigenmode 97 considers more local buckling of the plate, rather than web's, but demands greater applied stresses. Finally, the mode closer to critical mode has been chosen as the most suitable, because it introduces a stress level approaching more critical stress.

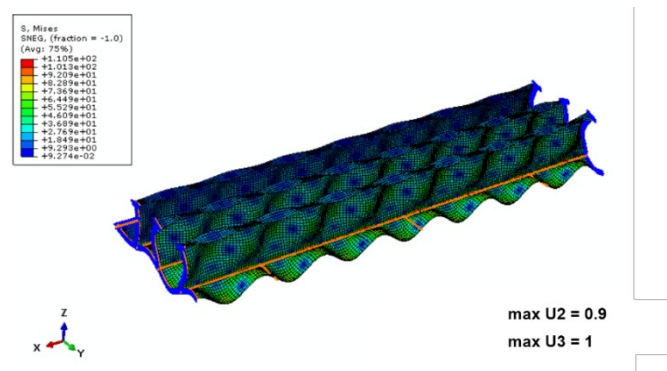

**FIG. 5.25**

Eigenmodes for pure axial compression (1-stiffener, 6-plate)

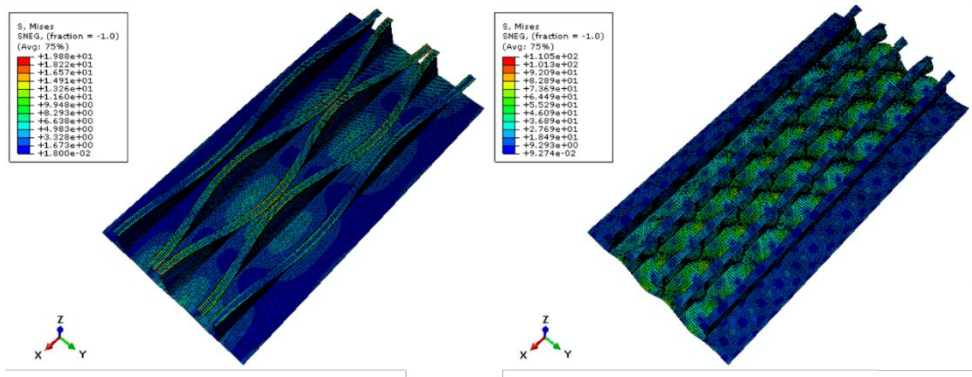
Transverse loads still result in eigenmodes with mixed local buckling on both the web and the plate, so every eigenmode contains a significant uncertainty. This means that although the web provides strength to the plate, it still tends to buckle more as a plate than as a stiffener.

Again, the same assessment procedure will be followed. The basic criterion that should be satisfied refers to web's deformations, which should not be overestimated compared to the plate. Furthermore, a well-distributed buckling mode on the whole plane of the plate should be preferred.

An example of satisfactory (local) buckling conditions dominating on the plate could be visualized by making a cut in y plane. The ratio between the displacements in transverse and vertical directions does not overestimate stiffener deformations, whereas along the whole surface of the plate symmetric half waves are formed. Due to the strong interaction of the plate to the web and vice versa, web also develops the same number of half waves in its surface.

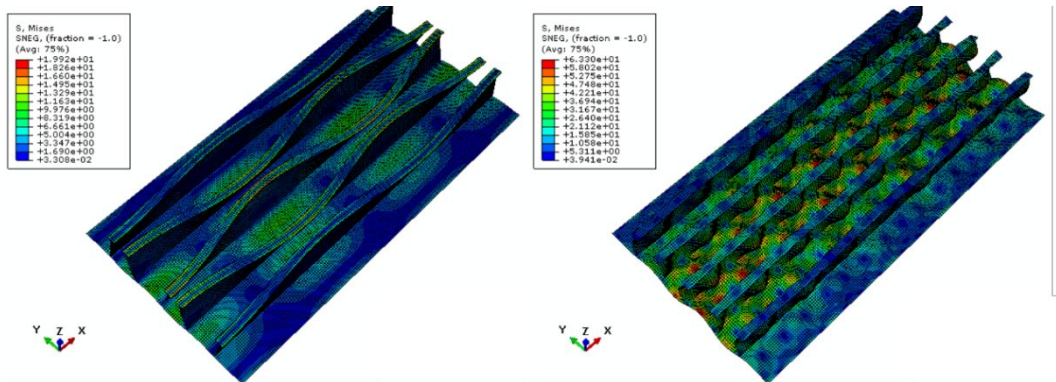

**FIG. 5.26**

Free cut - Stress conditions describing local plate buckling for 20% biaxial compression



**FIG. 5.27**

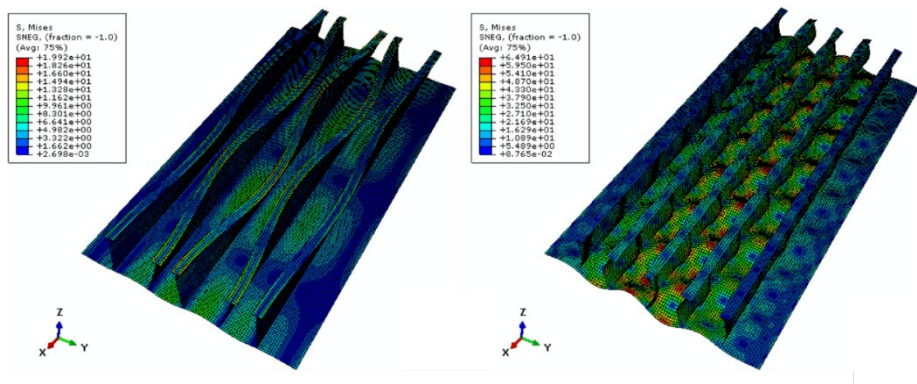
Eigenmodes for 20% biaxial compression (1-stiffener, 82-plate)



**FIG. 5.28**

Eigenmodes for 40% biaxial compression (1-stiffener, 25-plate)

Next, lateral pressure set as a preload will be applied. Stiffeners are still prompt to bend along the longitudinal direction first. What characterizes this case as more peculiar is that bottom pressure amplifies local plate buckling, making existing deformations greater than the web's. As a result, local plate buckling pattern is more evident than in previous modes. However, webs, except from local deformations on their plane, attain some rotational flexibility along their strong axis.


**FIG. 5.29**

Eigenmodes for lateral pressure as a preload (1-stiffener, 25-plate)

Stiffeners are proved weaker, so the structure is prompt to collapse due to their torsional buckling. Critical elastic buckling stresses illustrate small magnitude variations for each loading case, with a slight decrease as loading complexity increases, but in general, it could be assumed that stiffeners are so sensitive that fail approximately at a similar stress level.

It should be highlighted that there is a great difference between the critical stresses and the demanded stresses that could provoke plate buckling. Especially for high transverse loadings lateral pressure makes no difference on the collapse process of the model.

	Eigenmode	Eigenvalue	FEA elastic buckling stress (MPa)
pure axial compression	1 (stiffener)	8486.6	386
	6 (plate)	10468	476
20% stress ratio	1 (stiffener)	8287	377
	82 (plate)	14695	668
40% stress ratio	1 (stiffener)	7564	344
	25 (plate)	10448	475
constant pressure	1 (stiffener)	7559	344
	25 (plate)	10447	475

**TABLE 5.4**

Elastic buckling stresses for each loading case of T-900

### Nonlinear Analysis

From nonlinear analysis it is shown that the structure is more possible to collapse close to the center. There, the stiffeners cannot carry the bending moment caused on the flanges and over

failure of the model is inevitable. When biaxial loads of varying magnitudes are applied, the failure shifts to the last transverse girder. Stiffeners rotate and induce the plate to fail locally due to their interaction.

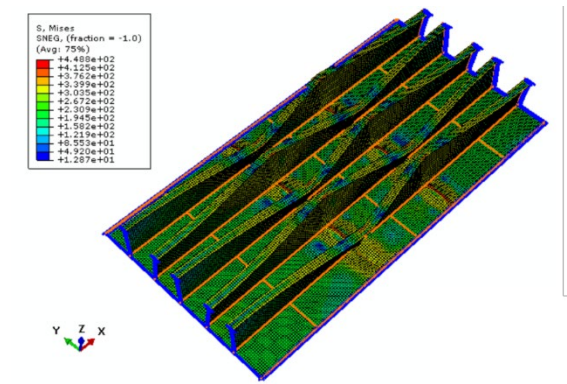


**FIG. 5.30**

NLA –Collapse due to pure axial compression

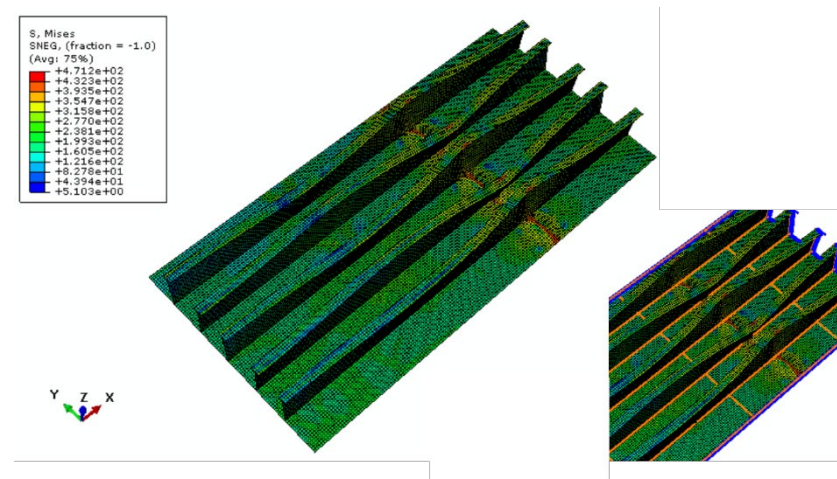


**FIG. 5.31**

NLA –Collapse due to 20% biaxial compression

It is remarkable that under pressure conditions, after bifurcation load is reached LPF will not drop immediately, but will follow a stable path and fall smoothly afterwards. That is probably caused because of the presence of a constant lateral pressure that will lengthen the postbuckling response of the structure.

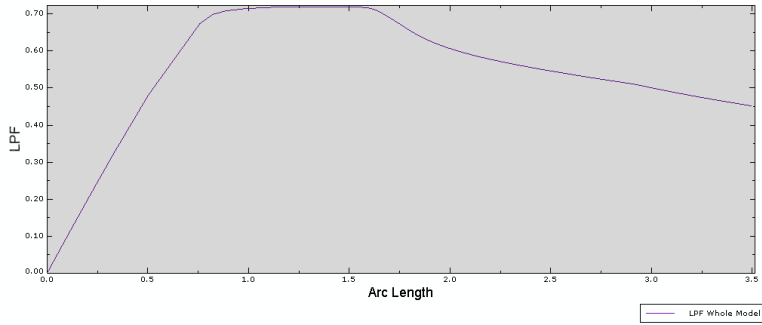


**FIG. 5.32**

Load proportionality factor when pressure acts at the bottom of T-900

The location of the failure is also dependent of the existence of pressure conditions. Now, yielding of the stiffeners close to the middle transverse girder induces collapse due to their torsion. In addition, the maximum displacements are caused by the bending of the flanges, while the plate gets insignificant deformations.

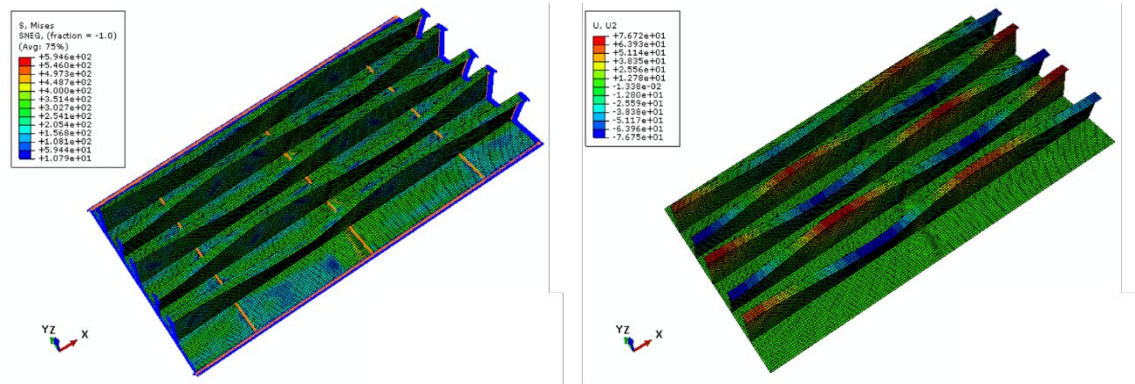


**FIG. 5.33**

Von Misses stresses and displacements in transverse directions when pressure conditions exist

### Ultimate Buckling Capacity of T-900

As shown by eigenvalue analysis, this type of stiffeners is weak and tend to fail in torsion first, caused by their big height compared to flange width. Therefore, the stiffener tends to behave more like a plate than as a column and overall buckling precedes local buckling. Additionally, the moment distribution developed close to the upper flange cannot be equalized by the torsional rigidity of the stiffener itself.

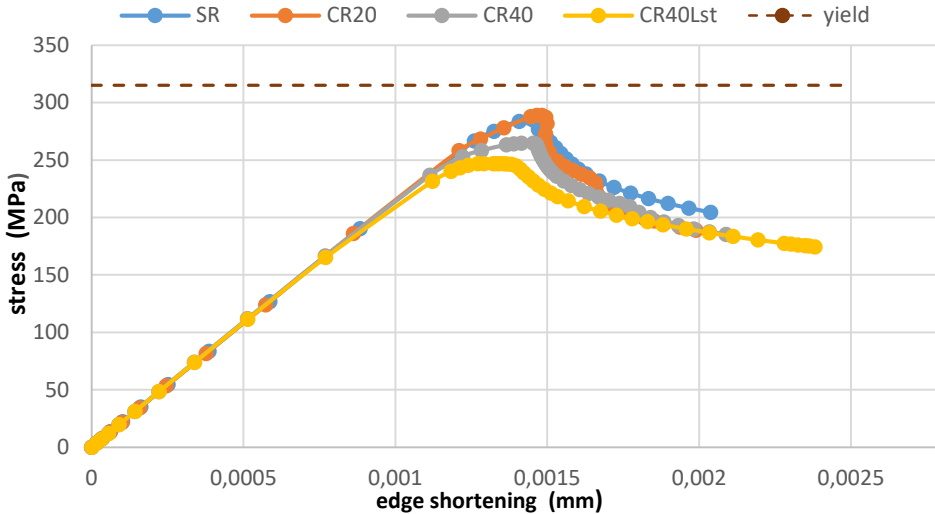


**FIG. 5.34**

Ultimate buckling capacity of panel T-600

Ultimate torsional buckling capacity for each load case validates that overall buckling, with overturning of the stiffeners dominates over local plate buckling. Generally, axial and moderate biaxial load conditions maintain the same ultimate capacity, whereas higher transverse loads and lateral pressure weaken the module and the structures proves to have lower capacity, therefore it buckles in torsion easier.

#### 5.2.4 Proposal Verification with FEA

An overview of the ultimate torsional buckling capacity for different heights of stiffeners of T-section is presented below. All geometric dimensions of the profiles remain the same, while the height of the stiffener increases.

It is obvious that as the height of the web increases, the torsional buckling capacity of the stiffener decreases. Hence, high stiffeners are more flexible in rotation to their longitudinal axis and as a result overall buckling due to collapse of the stiffeners precedes plate local buckling. On the other hand, stiffeners of a height 200-300 mm fail locally in plating before webs get effects.

Furthermore, it is proven that the results from FEA coincide at a high accuracy with those emerging from Closed Form Methods, proposed for the evaluation of torsional buckling behavior. For intermediate heights numerical methods tend to be more conservative, but in general it could be stated that both methods estimate ultimate buckling capacity reliably.

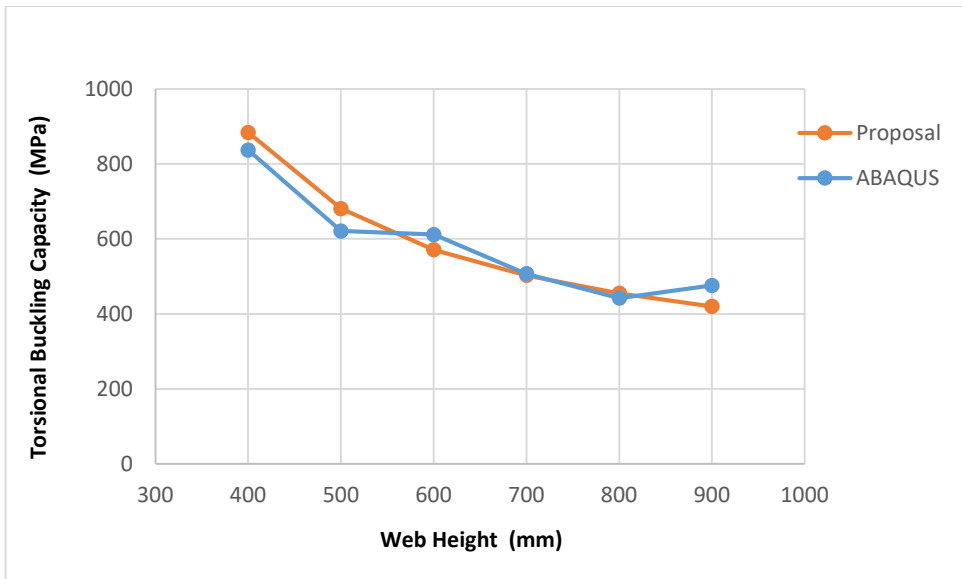


**FIG. 5.35**

Ultimate buckling capacity FEM-IACS verification

### 5.3 Panels with Attached Flatbars

Another type of stiffener that could be found attached to a plate is a flatbar, a structural component with no flange. Assuming that the profile of the stiffener is a rectangular section of a beam, the web could deliver shear stresses from the plate adequately, but due to flange absence not the induced bending moments. Flatbar is more prompt to buckle as a plate, with a number of half waves close to its aspect ratio,  $a = \frac{3200}{700} = 4.6$ , that is four to five half waves. Consequently, although torsional buckling in one half wave along the girder span is not an expected formulation like with T-stiffeners, different loading conditions are proved determinant for its occurrence.

During nonlinear analysis, tolerance levels corresponding to the maximum displacements that the plate and the stiffeners could take are 3.5mm and 3.2mm respectively.

#### 5.3.1 Finite Element Analysis of Flatbars

##### Linear Analysis

Flatbars of a varying height of 250 to 400 mm were examined. For this range, during pure axial compression all stiffeners buckle by rotation around x axis. Simultaneously, this web rotation interacts with the attached plating, forcing it to fail locally on an equal number of half

waves. The lack of resistance in bending, due to no upper flange, forces stiffeners to form in four to five half waves between each girder span.

Under such conditions, a mode with pure torsional buckling of the stiffeners in one half wave is impossible to be traced. In other words, webs are unable to deliver bending moments created by the plate and fail due to their interaction. Thus, only local buckling would be utilized to describe initial deformations of the plate and web (Fig. a).

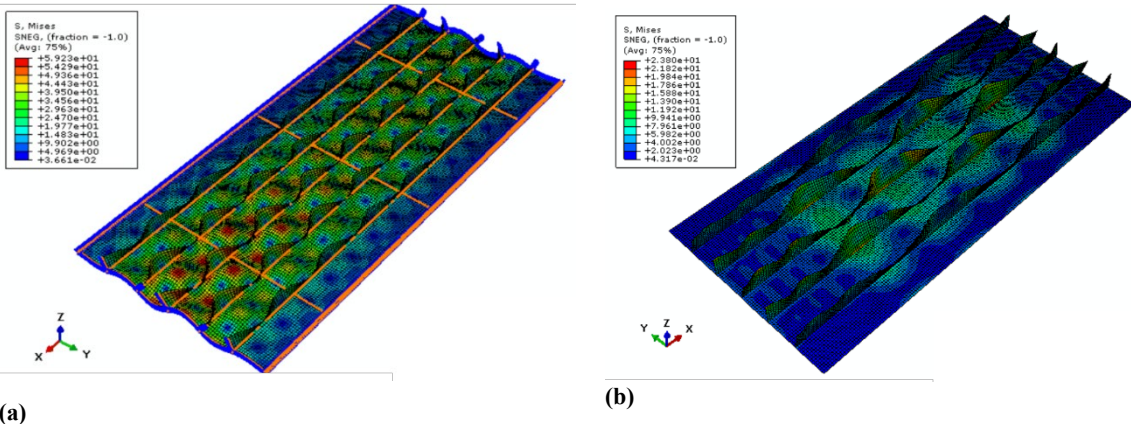


**FIG. 5.36**

(a) Pure axial compression of flatbars, (b) Pure axial compression of F-400 mm (eigenmode 66)

On the other hand, at the highest web of 400 mm, torsional buckling of the webs dominates, but only at stress levels significantly higher from critical. Stiffeners rotate in one half wave along their longitudinal axis and plate appears small deformations. However, in reality such failure will occur once more due to local plate buckling prior to rotational failure of webs.

The buckling pattern alters drastically when transverse loads are added. Still, plate is more susceptible to fail locally first, but stiffeners become more sensitive in torsion. After certain stress levels, plate could buckle “in and out” in one half wave, inducing the stiffeners to deform similarly. For low transverse loads, torsional buckling mode is encountered at high eigenmodes, thus high stresses, whereas substantial transverse loads transfer these modes closer to critical.

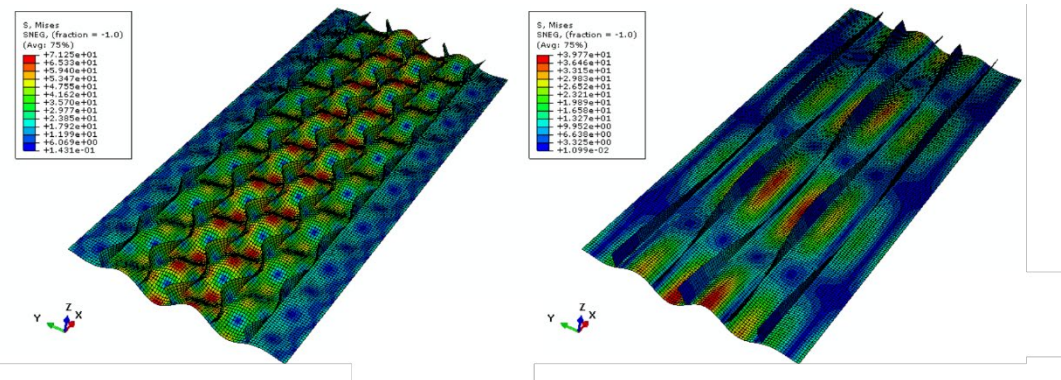


**FIG. 5.37**

Eigenmodes for 20% biaxial compression (7-plate, 42-stiffener)

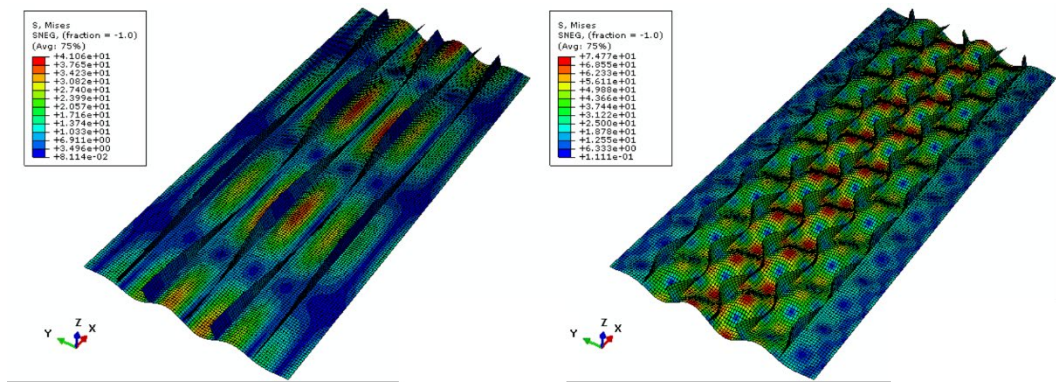


**FIG. 5.38**

Eigenmodes for 40% biaxial compression (7-stiffener, 20-plate)

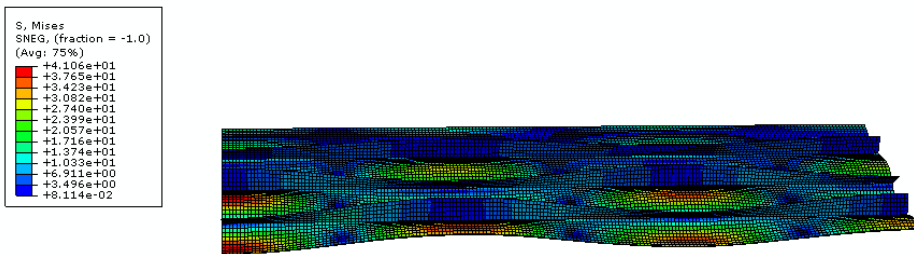


**FIG. 5.39**

Longitudinal cut of the panel showing “in and out” deformations of the plate

Presence of lateral pressure leads to overall grillage buckling. It strengthens plate capacity and induces it to buckle in one half wave between girders. At the same time, plate puts a strain on stiffeners, forcing them to buckle at the same pattern. These deflections are accompanied by bending of transverse girders, while maintaining symmetry conditions at short edges.

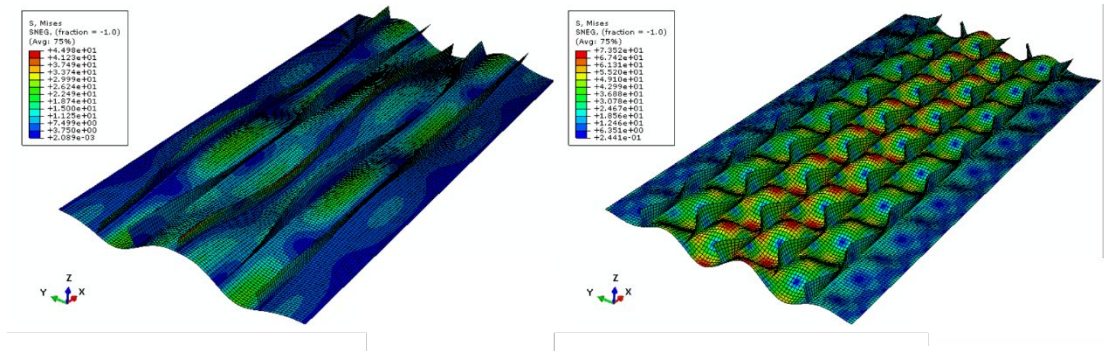


**FIG. 5.40**

Eigenmodes for lateral pressure as a preload (1-stiffener, 21-plate)

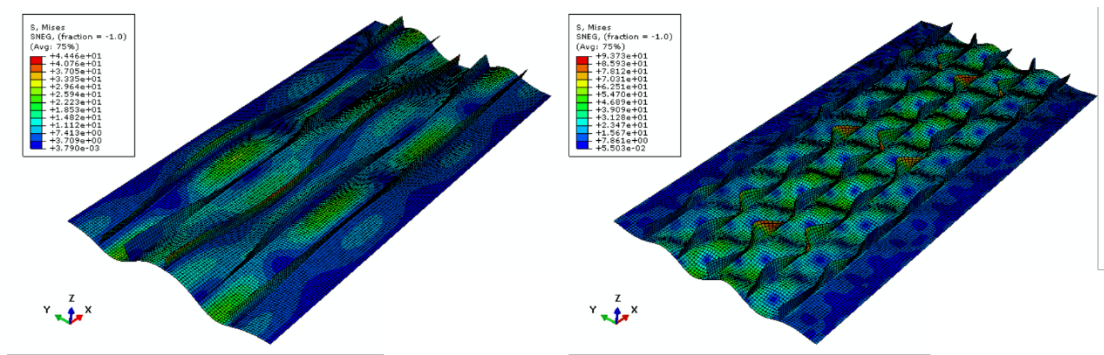


**FIG. 5.41**

Eigenmodes for proportionally increased lateral pressure (1-stiffener, 20-plate)

According to the table below, each ascending loading case inflicts to descending critical (elastic) buckling stresses. Also, the dominant buckling pattern is indeterminable and could not be predicted easily before the analysis.

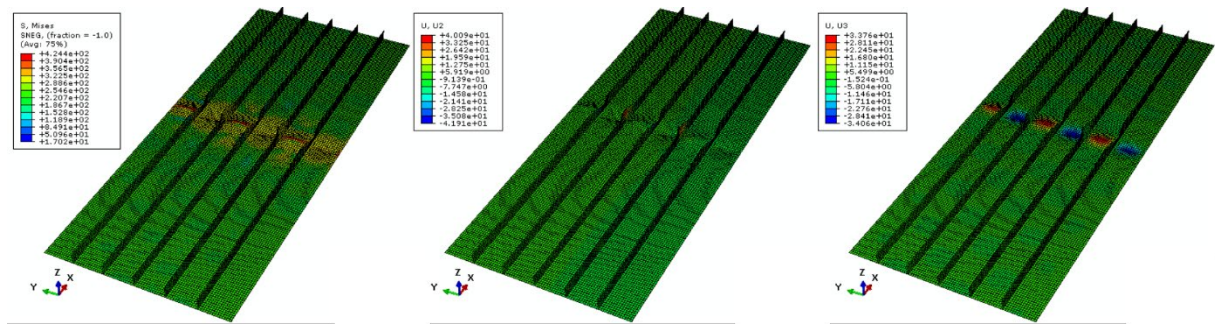
	Eigenmode	Eigenvalue	FEA elastic buckling stress (MPa)
pure axial compression	1 (plate)	16738	761
20% stress ratio	1	13968	635
	7 (plate)	14765	671
	42 (stiffener)	20055	912
40% stress ratio	1	10958	498
	7 (stiffener)	11342	516
	15 (plate)	13123	597
increasing pressure	1 (stiffener)	8567.9	389
	20 (plate)	9930.1	451
constant pressure	1 (stiffener)	9236.8	420
	21 (plate)	13310	605

**TABLE 5.5**

Elastic buckling stresses of F-250

### Nonlinear Analysis

As mentioned in eigenvalue analysis, plate buckling modes dominate when axial and moderate biaxial loads are present. Indeed, the results of nonlinear analysis prove that the model fails at a certain region due to evolving plate deformations, forcing the webs to fail local at the same place. For both, the failure localizes either close to the girder (Fig.5.42) or at the unloaded short edge of the panel (Fig.5.43)


**FIG. 5.42**

Von Misses stresses and maximum displacements in pure axial compression

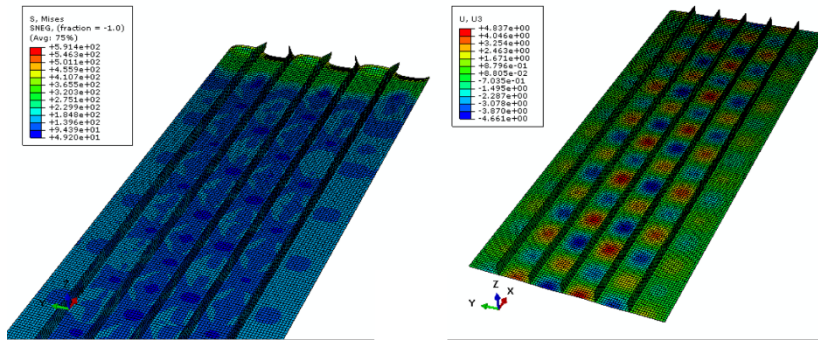


**FIG. 5.43**

Von Misses stresses and maximum displacements in 20% biaxial compression

When more significant biaxial magnitudes act, a more complex procedure evolves. Failure regions delocalize and all areas close to transverse girders become potential to collapse. Even though linear analysis modes favor web torsion, nonlinear analysis evolves local buckling of both plate and webs as the dominant buckling pattern.

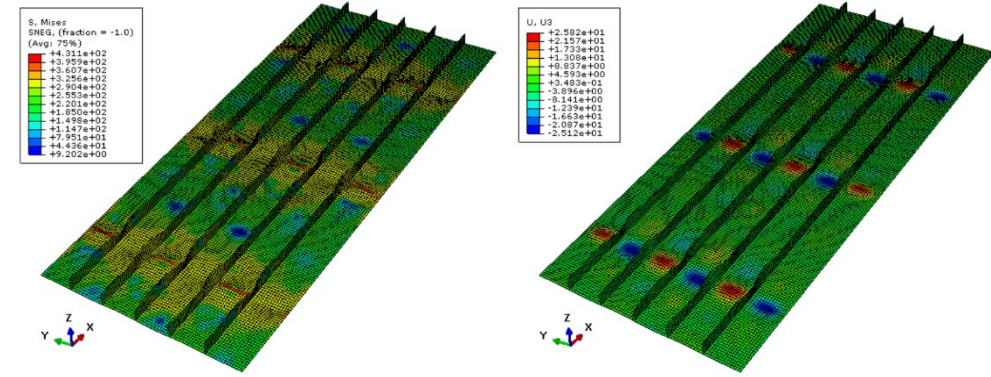


**FIG. 5.44**

Von Misses stresses and maximum plate displacements in 40% biaxial compression

Overall grillage buckling due to pressure is verified by nonlinear analysis too. Both approaches develop identical failure mode, with a difference that increasing pressure localizes failure at one girder whereas constant pressure from the beginning leads to overall collapse of the model. This is mainly owed to the maximum values pressure reaches during the two paths. In the first case, the model buckles before reaching its maximum value, forces concentrate in one region and the whole girder collapses. On the other hand, the analysis begins with an already maximum pressure, thus models collapse is driven to yield before buckling.

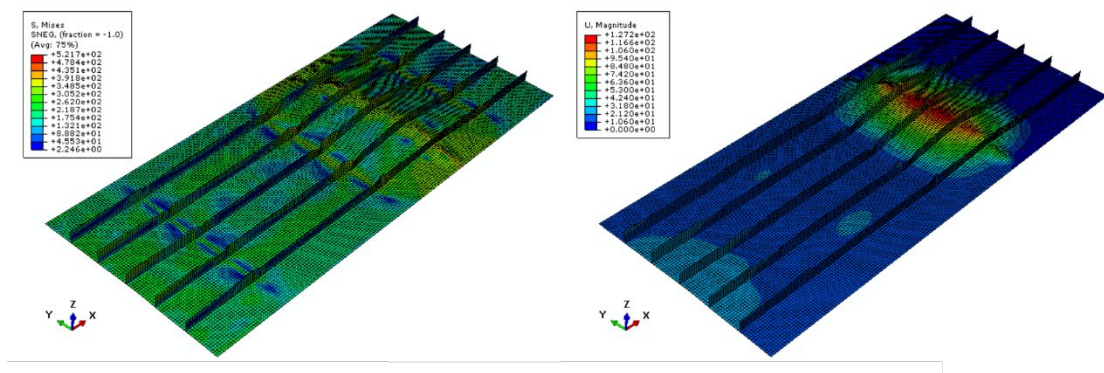


**FIG. 5.45**

Von Misses stresses and maximum displacements when increased pressure applies

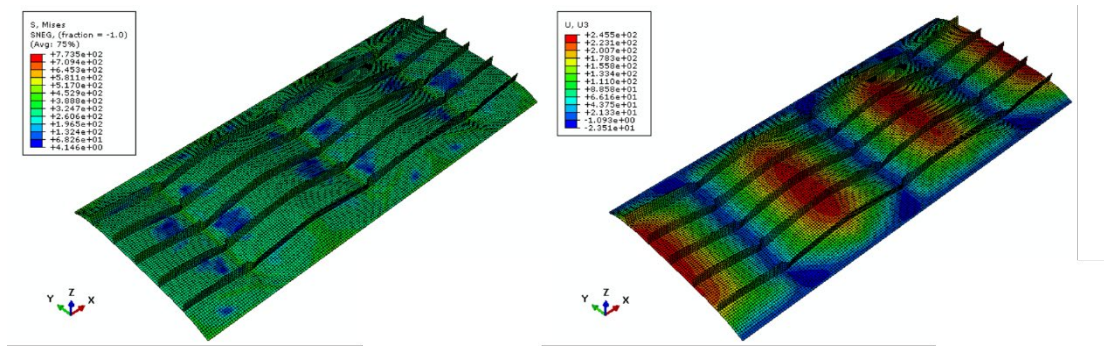


**FIG. 5.46**

Von Misses stresses and maximum vertical displacements when constant pressure conditions exist

### 5.3.2 Ultimate Buckling Capacity of Flatbars

While all modeled stiffened panels proved to have similar torsional behavior, the ultimate capacity of 250 mm webs under different loading scenarios is cited. Furthermore, 250 mm is a common stiffener height in more ship and offshore applications.

Eigenmode patterns illustrate an intense alternation of the emerging collapse modes, highly dependent on the type of loading. In general, local plate buckling is dominant when modest loads practice, but more complex combinations could overturn existing conditions. Especially under pressure conditions, it could be difficult to prevent the structure from overall grillage collapse. Nonetheless, it is not feasible to foresee the possible plane of failure as each case demonstrates special behavior.

In reality, when geometrical and material nonlinearities are considered, local plate buckling is the dominant collapse pattern that each model follows.

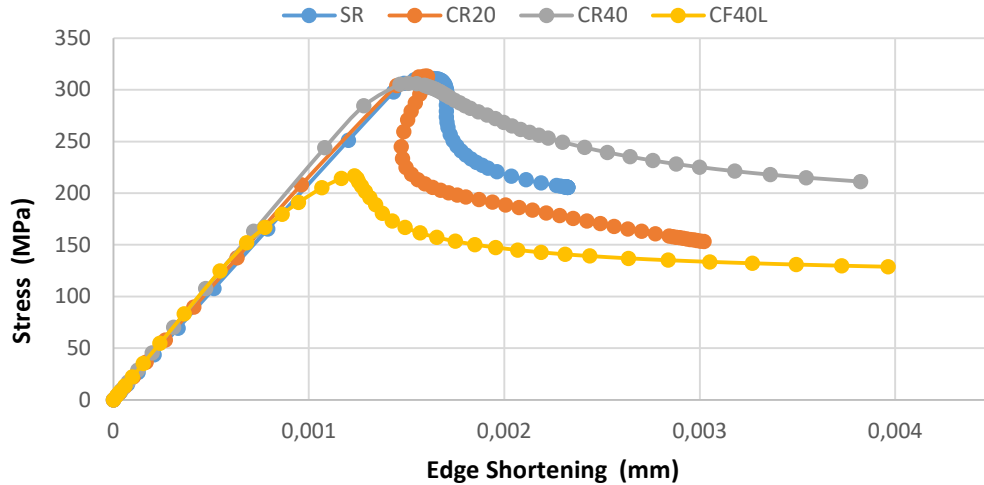


FIG. 5.47

Ultimate Buckling Capacity of F-250

For the examined web heights, the proposed formula estimates ultimate buckling capacity in torsion. FEA proves that local plate buckling will be the determinant failure factor, therefore the equivalent stresses from FEA could not be traced. Nonetheless, even though torsional buckling capacity is overestimated and will never be reached in reality, the results are presented in the following figure for flatbars forming four to five halfwaves at each girder span.

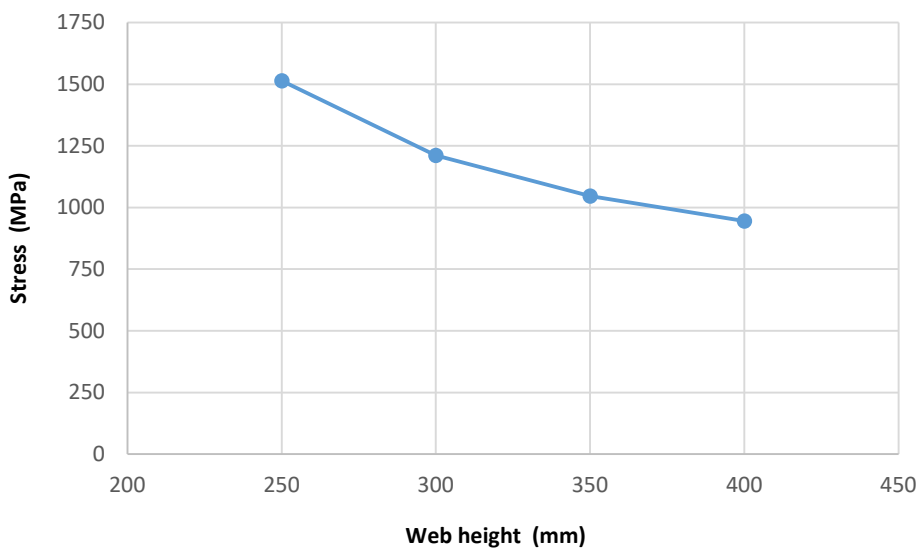


FIG. 5.48

Ultimate torsional buckling capacity of flatbars (Proposed formula)

## **6. Conclusions**

Classifications societies, ship/offshore designers and yards are under a continuous research of introducing new methods to estimate the ultimate capacity of primary structural elements. Buckling and even more torsional buckling is a complex and ambiguous aspect, that demands technical knowledge and engineering experience. Research on the ultimate strength of stiffened panels for ship and offshore structures continues to receive worthwhile attention, for an efficient design combined with safety.

Over the last decades, many engineers were occupied on the explanation of torsional buckling behavior, developing theories based on analytical solutions. Nowadays, to simulate buckling of thin-plated structures, both analytical and numerical methods could be applied.

During this project, finite element analysis (FEA) was the selected numerical method for the testing of stiffened panels. The simulation of their structural behavior, considering both material and geometrical nonlinearities, was a complex procedure. Reasonable accuracy was achieved in terms of the expected torsional buckling sensitivity of the modules, due to proper meshing, element type, boundary and loading conditions. The selection of the most representative boundary conditions for the plate and the stiffeners was a major factor, so as to reciprocate the conditions under which stiffeners exposed to torsion exist. Therefore, the symmetry conditions set at the compressed edges or the fictional existence of transverse girders restricting webs motion in transverse direction, formed the appropriate environment, under which stiffened panels subjected to compressive stresses could buckle in torsion. However, results of FEA are obtained only numerically, and consideration on physical meaning of the calculated results is necessary.

FEM is proven to be a useful tool for the evaluation of the buckling behavior and ultimate capacity of stiffened panels. The parameters which effect the strength of a stiffened panel under compression are various, including geometry, stiffener type, material properties, support conditions and loading patterns. The use of FEM is distinguished in two main categories: linear/eigenvalue and nonlinear analysis. A detailed explanation of each method's contribution to buckling and postbuckling behavior of the tested models is illustrated.

During eigenvalue analysis, the revolving failure modes of the structure were presented directly. The preference on that analysis for a fast model checking was due to the simplicity of its modelling definition and of the extracted results. The emerging eigenmodes gave a complete overview of structure's collapse modes, showing an inclination towards the dominant buckling patterns. The selection of the appropriate modes that could illustrate more

accurately plate local buckling or torsion of stiffeners was complicated, as almost always an interaction between different deformations occurred. Eventually, the selection was mainly based on eigenvalues with magnitudes close to critical buckling stresses. Furthermore, the fact that the preferred modes should not magnify the deformations at one of the two members (plate or stiffener), defined also the critical eigenmodes. However, this procedure was not always straightforward.

Nonlinear approach required some additional settings but gave enormous post-processing possibilities. Its indissoluble relation to linear analysis, due to the superposition of the chosen eigenmodes to attain geometrical imperfections of the new “imperfect” model, confirmed the demanded critical thinking during eigenvalue selection. Eventually, it was feasible to calculate the shortening of the compressed edges, which generally increased while more complex loadings applied.

For both stiffener types, dominant loading conditions determine the response of the structure and the evolving failure modes. Generally, T-stiffeners deploy their maximum capacity when pure axial or moderate biaxial forces (10%-20%) act normal to their planes. For same heights, variation between such loadings show no significant effect on the ultimate capacity of the model. Only when biaxial loads higher than 40% are applied, the panel becomes weaker to withstand the bending moments caused by torsion. The effect of torsion is magnified more when lateral pressure is added. Increasing lateral pressure is more favorable compared to a constant lateral load, which eliminates the capacity of the stiffened panel appreciably. In the first case, web stiffness maintains in and out deformations at the bottom while a constant pressure results to inward deformations that weaken the webs. Therefore, the chosen loading path of T-stiffeners during lateral compression has proven important for the final evaluation of their strength.

The height of T-stiffeners also determines their ultimate buckling capacity. Short webs of 200-400mm are strong in torsion and high loads should be applied in order to warp them. Therefore, local buckling develops before torsional buckling of the webs. This pattern reverses for stiffeners of 450-700mm. Such web heights, where the upper flange has a significant distance from the shear center, rotate easier the stiffener and torsional buckling failure develops first. Stiffened panels with higher webs are considered more as two attached plates. The buckling behavior of the webs is similar to a plate, which justifies why collapse due to local buckling of the web dominates.

Examination of flatbars showed that they bend around their weak axis easily under any force combination, proven unable to develop any bending resistance. For a flat plate the warping rigidity is negligible, therefore their rotational rigidity is zero. The absence of the upper

flange, which cannot now deliver bending moments, amplifies their torsional flexibility, forcing them to follow the buckling pattern of the plate. Thus, torsion induces bending of the web because of the plate, but not as a pure effect. This justifies the reason the examined flatbars buckle at an equal number of half waves as the plating. Therefore, the lowest elastic buckling stresses corresponding to the torsional mode of buckling with no rotation restraint from the plate are very close to the local buckling strength of the plate. That buckling pattern alternates only when significant transverse magnitudes are added to the model (40%). In that case, but only over much higher than critical elastic stress levels, flatbars tend to approach the torsional behavior of T-stiffeners, warping in one half wave along each transverse girder span. However, in reality they would collapse at lower applied thrust. When both concepts of lateral pressure are applied, the stiffened panel is unable to resist and interframe flexural buckling develops. Their deficiency in torsional buckling made it impossible to validate the results of FE analysis to the proposed formulas.

On the other hand, the IACS proposed analytical formulas assume proper functions for the produced buckling deflection modes, which are more complex to process and understand and demanding deep knowledge of principal theories. Although their application is limited to relatively simple problems such as elastic behaviors under fundamental loads and boundary conditions, the solutions having physical meaning can be obtained explicitly. The accurate solution, however, cannot be obtained if the assumed deflection functions are not proper, as happened in the case of flatbars.

There, the variables describing the deflection function of flatbars, considered the calculation of warping stiffness of the web, when in reality flatbars present zero warping restraint. Thus, torsional buckling stresses were overestimated. Moreover, as FEM highlights, a pure torsional buckling pattern is hard to be developed, because flatbars fail due to lateral bending and can never reach such stress levels that torsional buckling precedes lateral bending. Therefore, for such cases formulas are proven inaccurate and distort the real behavior of flatbars. On the contrary, the evaluation of torsional buckling capacity for T-stiffened panels is validated adequately by numerical results.

An important deficiency of the proposed formula could be that the ultimate torsional buckling capacity of stiffened panels is based on the assumption of pure axial compression. Even though warping stresses contain more complex loading cases, this formula fails to incorporate the effect of combined in-plane loads or lateral pressure and, as a result, the extracted values overestimate the ultimate capacity of the stiffened panel. Additionally, the ultimate capacity refers to elastic buckling stresses, which means that a more conservative estimation is made.

To conclude, the main difference of flatbars and T-stiffeners is owed to the existence of the upper flange. As it is known, webs deliver shear stresses while flanges deliver bending moments. Therefore, the torsional buckling capacity of a stiffened panel depends on the shape of the attached stiffener. For the design of structures with high resistance in torsion, stiffened panels with attached T-stiffeners of intermediate height are mainly preferred, even though this is not the rule. Various parameters should always be checked, such as the forces dominating at the primary members of the structure and the thickness of the structural members. In many cases, increasing the thickness of the web or reducing the breadth of the flange could reinforce stiffener's durability in torsional effects.

## References

- [1] Timoshenko S, Gere J. Theory of elastic stability. McGraw-Hill Kogakusha. (1961); 212-232
- [2] Fujikubo M, Yao T. Elastic local buckling strength of stiffened plate considering plate/stiffener interaction and welding residual stress. (Mar Struct 1999); 543–564.
- [3] Owen F. Huges and Jeom Kee Paik. Ship Structural Analysis and Design
- [4] Bleich F. Buckling Strength of metal structures. (1952)
- [5] Amdahl J. Buckling and Ultimate Strength of Marine Structures, Lecture notes, Ch. 2-3 (2018)
- [6] DNVGL-CG-0128. Buckling.
- [7] IACS Common Structural Rules for Bulk Carriers and Oil Tankers. Ch.5 (2019)
- [8] Timoshenko S, Gere J. Theory of plates and shells. McGraw-Hill Higher Education. (1964)